Permeation of CO_2 and N_2 Through Glassy Poly(Dimethyl Phenylene) Oxide (PPO) under Steady and Pre-Steady State Conditions

Marielle Soniat [a,b], Meron Tesfaye [c,d], Amirhossein Mafi[e], Daniel J. Brooks [e], Nicholas D. Humphrey [e], Lien-Chun Weng [a,d], Boris Merinov [e], William A. Goddard, III [e], Adam Z. Weber [a,c], and Frances A. Houle [,a,b]*

a Joint Center for Artificial Photosynthesis, Lawrence Berkeley National Laboratory, Berkeley, CA 94720, USA

b Chemical Sciences Division, Lawrence Berkeley National Laboratory, Berkeley, CA 94720, USA

c Energy Storage and Distributed Resources Division, Lawrence Berkeley National Laboratory, Berkeley, CA 94720, USA

d Department of Chemical and Biomolecular Engineering, University of California, Berkeley, CA 94720, USA

e Materials and Process Simulation Center (MSC), Beckman Institute,
California Institute of Technology, Pasadena, CA 91125, USA

Abstract

Glassy polymers are often used for gas separations because of their high selectivity. Although the dual mode permeation model correctly fits their sorption and permeation isotherms, its physical interpretation is disputed, and it does not describe permeation far from steady state, a condition expected when separations involve intermittent renewable energy sources. To develop a more comprehensive permeation model, we combine experiment, molecular dynamics, and multiscale reaction-diffusion modeling to characterize the time-dependent permeation of N_2 and CO_2 through a glassy poly(dimethyl phenylene oxide) (PPO) membrane, a model system. Simulations of experimental time-dependent permeation data for both gases in the pre-steady state and steady state regimes show that both single-mode and dual-mode reaction-diffusion models reproduce the experimental observations, and that sorbed gas concentrations lag the external pressure rise. The results point to environment-sensitive diffusion coefficients as a vital characteristic of transport in glassy polymers.

Introduction

Non-porous polymeric materials are commonly used as membrane separators for gas purification, reverse osmosis, and pervaporation, among other applications.[1-5] For gas transport through any non-porous polymer, the widely accepted model for permeability, P, is the solution-diffusion model, which gives a phenomenological description of the permeability as the product of the solubility coefficient, S, and the diffusion coefficient, D, at steady state, i.e.,[6-7]

	$P = DS$	(1)

In the typical use of the solution-diffusion model, the diffusion coefficient is assumed to be the proportionality constant between the flux and the concentration (or chemical potential) gradient; as such, it should be constant so long as the material properties and temperature are constant (Case I diffusion).[7-8] The diffusion rate may also depend on changes in the bulk polymer morphology upon exposure to permeants (Case II diffusion) or a combination of concentration gradient and polymer morphology change (anomalous diffusion).[8] In most studies, interactions between the polymer and permeant causing, changes in polymer morphology over time (e.g., aging) and inhomogeneity in polymer morphology (e.g., different density in the surface region) are not included explicitly using appropriate variables, but instead are subsumed into the reported D.[8-10] This limits the predictive capabilities of the solution-diffusion model.

The standard application of the solution-diffusion model is as a steady-state model, intended to describe situations where the membrane properties and external conditions are constant. In cases where the polymer properties change upon initial exposure to a permeant or where the external permeation concentration is changing (e.g., produced in systems driven by intermittent, renewable energy sources such as sunlight or wind[4-5, 11-12]) such non-steady state permeation cannot be predicted in a mechanistic way by the solution-diffusion model. In contrast, physically-based, mechanistic descriptions of permeation that capture time-dependent physical and chemical processes will provide computational frameworks that are predictive, afford greater scientific insight across length and timescales, and apply to a wider range of permeation conditions. In previous studies,[11-12] we have reported such descriptions for gas sorption and permeation involving rubbery polymer membranes and sorption of aqueous solutions of methanol by Nafion. Those works allowed a multiscale simulation framework for transport of weakly and strongly interacting permeants to be developed. Although the systems studied are quite different chemically, the framework has mechanistic elements common to both: interfacial transport, bulk diffusion, and time-dependent solute concentrations. In this paper, we extend the computational framework to represent permeation through polymeric glasses, drawing on mechanisms proposed in the literature.[13]

A major difference between rubbery and glassy polymers is the presence of excess fractional free volume (FFV) in the glassy state due to

kinetically trapped molecular chains.[14-15] While FFV exists in all materials,[16-18] the excess FFV is proposed to play a special role in sorption and diffusion within glassy polymer materials.[19] An increase in FFV has been shown to correlate with an increase in permeability and diffusion coefficients across a wide variety of glassy polymer compositions.[20] Positron annihilation lifetime spectroscopy (PALS) confirms that a discontinuity in the temperature dependence of the size of the void spaces, called free volume elements (FVE's), occurs at the same point as the discontinuity in the volume,[18] indicating that the excess FFV is mainly incorporated by increasing the size of the FVE's.[21] The presence of excess FFV led to the proposal of the dual mode model, in which the total permeant solubility is given by two different modes within the polymer.[13] The first mode is associated with sorption into the polymer matrix in the same manner as Henry's Law sorption into rubbers or liquids, and is often referred to as the dissolved mode. The second mode is associated with Langmuir-type adsorption to the internal surfaces of the FVEs, and has a non-linear relationship to the external pressure.[19] The equation for the total pressure-dependent concentration of the gas, $[X](p)$, within a glassy polymer is

$$[X](p)=S_d p+\frac{S_L b_L}{1+b_L p}p \quad (2)$$

where p is the external pressure, S_d is the dissolved solubility coefficient, and S_L is the Langmuir solubility coefficient, and b_L is the affinity parameter.[19] Commonly, separate diffusion coefficients are associated with each mode on

the basis of the dual mobility partial immobilization model,[22-23] such that the permeability isotherm[24] is given by

$$P = S_d D_d + \frac{S_L b_L}{1 + b_L p_{up}} D_L \quad (3)$$

where D_d is the diffusion coefficient associated with dissolved sorption, and D_L is the diffusion coefficient associated with Langmuir sorption. In total, five fitting parameters are used to describe the observed decrease in permeability and the decreasing effect on marginal sorption with increasing pressure.[19, 24] While the mathematical formulas for dual mode sorption fit the isotherms well, the physical basis for this picture has been called into question.[25-40] For example, the amount of CO_2 absorbed into poly(dimethyl phenylene oxide) (PPO) via the Langmuir mode is greater than that of N_2,[41] even though N_2 has the smaller critical volume,[16] defined as the volume occupied by a molecule at the critical point in the phase diagram. The lesser amount of N_2 sorbed into PPO contrasts with expectations from simple space-filling arguments. Additionally, molecular dynamics (MD) simulations indicate that voids are short-lived, and that diffusion in both rubbery and glassy polymers is controlled by jumps between FVE;[35-36] this indicates that the contribution of the free volume to permeation may not be substantially different from the rubbery case.

Herein, we investigate the applicability of modeling permeation through glassy polymers with both single mode and dual mode models under both non-steady state and steady state conditions. We investigate the permeation of poly(dimethyl phenylene oxide) (PPO) by an inert gas, N_2, and

a plasticizing gas, CO_2. Physically based, multiscale simulations of time- and pressure-dependent permeation data provide a sensitive test of a permeation mechanism. Reaction-diffusion simulations, informed by molecular dynamics calculations and experimental data, are performed for comparison to experimental measurements made for this work. The results show that models using either single or dual modes can describe gas permeation through glassy PPO when the experimentally measured pressure-dependent solubility and diffusion coefficients are used. However, the time for the maximum gas uptake by the glassy polymer delayed relative to the time for the upstream pressure rise, rather than being instantaneous as in rubbery polymers.[12] The basic framework developed in this work will serve as a foundation for the future study of permeation through polymer electrolyte membranes (PEMs) formed from functionalized PPO that are under development for solar fuels applications under steady-state and non-steady state conditions.

Methods

1. Experimental

Complete time-dependent permeation data were measured for PPO as a function of pressure for N_2 and CO_2. Materials preparation and characterization, measurement methods, and data analysis are described in this section. The permeation apparatus has been described previously.[12]

1A . Preparation of PPO Membranes

Powder poly(2,6-dimethyl-1,4-phenylene oxide) (PPO) was purchased from Sigma Aldrich (St. Louis, MO) and dissolved in trichloroethane (ACS Reagent, Sigma Aldrich) at a ratio of 10% by weight. The solution was stirred continuously for 2 days and filtered with Millex PTFE filter (0.45μm, Millipore, Burlington, MA) to ensure removal of undissolved powder lumps and contaminants and to disperse large polymer aggregates that may have formed. The solution was then degassed for about 20 minutes in a vacuum desiccator to remove air bubbles formed during filtering process. The manufacturer-provided PPO material characteristics are powder density of 1.06 g/cm^3, glass transition temperature of 211ºC, and melting temperature of 268ºC.

PPO samples were cast on silicon wafers in 3 layers in a class 100 clean room. Silicon wafers (6-inch, silicon 100, p-type, Pure Wafer, San Jose, CA) were prepared by rinsing with deionized water, followed by blow drying with N_2, two rinses with isopropyl alcohol, and finally drying with N_2. Each wafer was placed on a hot plate at 373 K for 3-4 minutes to remove any residual alcohol from the surface of the wafer. The first layer of PPO was cast on a Silicon wafer and spun at 600 rpm for 200 s using a Laurell spin coater (Laurell Technologies Corp., North Wales, PA). The layer was dried at room temperature, then placed in a vacuum oven. Any trapped air pockets were removed by switching the oven between a nitrogen purge and vacuum 3 times for 20-40 s each, and then drying under vacuum at 120ºC. The second layer was cast on top of the first layer once it has cooled completely. The

same series of drying, purging, and vacuum drying were followed. The third layer was formed in the same manner as the second layer. The drying times for each layer are listed in Table 1. The final sample was cooled to room temperature, cut into small pieces, and removed from the silicon wafer. Data from 4 samples are reported in this work.

Table 1. Drying times after casting for each of the layers in the PPO sample.

Layer	Drying Time (min.)	
	Room Temperature	120°C in Vacuum
1	75	40
2	120	60
3	120	80

1B. Materials Characterization

The PPO film density was measured using helium gas pycnometer (AccuPyc II 1340, Micromeritics, Norcross, GA). Films were cut into small pieces and placed in sample cup (1 cm^3 total) in the pycnometer. Each sample was degassed 50 times to remove trapped air inside the cup, and the occupied volume is measured with 30 repeats/sample. The measurement was repeated 3 times. From the film density, the FFV was calculated using the Bondi method.[42-43]

The glass transition temperature was measured using dynamic scanning calorimetry (DSC 8000, Perkin Elmer, Waltham, MA). Samples were

placed in a DSC hermetic pan and subjected to a heating protocol of 3 heating steps followed by 2 cooling steps within the temperature window of 30-300ºC at 20ºC/min. The glass transition temperature was calculated from the 2nd and 3rd heating step and averaged over 3 samples. Crystallinity, χ_c, was calculated using the melting onset and peak temperature.[44]

1C. Permeation Measurements

PPO samples were placed in the permeation assembly, backed by a filter paper, and sandwiched between two flat aluminum supports. The aluminum supports allow for transport through a defined active area but do not alter the measured permeability. The sample assembly was then placed in the permeation cell for measurement.[45] All permeation experiments were performed at 35ºC. The sample was exposed to vacuum of 3 kPa or less for at least 10 hrs to remove any residual water or gas pockets. Initially, the downstream valve connecting the permeation cell to the vacuum pump was closed, and any slow pressure rise in the downstream volume, $(dp_{ds}/dt)_{leak}$, was monitored to test for leaks in the experimental apparatus. The sample was then exposed to dry N_2 or CO_2 gas (99.995% pure, Praxair, Danbury, CT) at the pressure of interest on the upstream side. Permeation through each of the 4 samples was measured for both gases at all pressures. The upstream pressure rise was recorded so that it can be included as part of the physical system in the simulation. The system typically takes 2-25 s to reach its final upstream pressure value, which ranges from 0-18 atm in this work. As gas permeates through the membrane, the pressure rise in the closed

downstream volume, (dp_{ds}/dt), was monitored. Once steady state was reached, signaled by a linear rise in downstream pressure over time, $(dp_{ds}/dt)_{SS}$, the permeability was calculated using the following equation,

$$P_m = \frac{Jl}{p_{up} - p_{ds}} = \frac{V_{ds} l}{\Delta p A R T}\left[\left(\frac{d p_{ds}}{dt}\right)_{SS} - \left(\frac{d p_{ds}}{dt}\right)_{leak}\right] \quad (4)$$

where P_m is the permeability of the membrane, J is the gas flux, l is the membrane thickness, Δp is the difference in upstream pressure, p_{up}, and downstream pressure, p_{ds}, A is the active area for flux measurements, V_{ds} is the downstream collection volume, R is the universal gas constant, and T is the temperature. This equation applies when $p_{up} >> p_{ds}$ and p_{up} is constant; these conditions are met in our experiments during steady state. Values for l, A, and V_{ds} are recorded in Table 2.

Table 2. Summary of experimental setup for each sample.

Sample	l	A	V_{ds}
	μm	cm^2	cm^3
1	32.25	0.970	41.73
2	22.42	0.495	41.73
3	19.39	0.495	41.73
4	19.39	0.495	41.73

1D. Calculation of Diffusion Coefficients

Sorption isotherms are fairly consistent across several literature studies of PPO,[20, 24, 41, 46] and so we assume that our samples also have the

same solubility as that reported by Toi *et al*.,[41] whose dual mode parameters are reported in Table 3. Permeability and therefore diffusivity vary more widely, and that is why we calculate the diffusion coefficients specific to our samples of PPO. For reference, literature values of sorption and permeability of CO_2 in PPO are reproduced in Supplementary Information (SI) Section 1.

Transport coefficients were calculated from the experimental data. In the first method, the apparent diffusion coefficient, D_{app}, was calculated using the standard single-mode solution-diffusion model (Eqn. 1). From the experimental permeability and the apparent solubility, S_{app}, at a given pressure p, the apparent diffusion coefficient, D_{app}, is given by

$$D_{app}(p)=\frac{P_m(p)}{S_{app}(p)} \quad (5)$$

where

$$S_{app}(p)=\frac{[X](p)}{p} \quad (6)$$

In the second method, the experimental permeability versus upstream pressure was fit to the dual mode model for permeation (Eqn. 3) with two adjustable parameters D_H and D_L.

It is commonly reported that the diffusion coefficient can be calculated independently from the lag time with the equation $\tau=l^2/(6D)$, where τ is the x-intercept in a plot of downstream quantity of gas vs. time. The time-lag equation was derived with the assumption that the upstream pressure increases from 0 to its steady-state value as a step function. In a real experimental apparatus, however, the upstream pressure takes some time

to increase, and at early times, the downstream pressure vs. time data are dependent on the functional form and rate of the upstream pressure increase. When the lag time method was used to calculate D from our experimental data, 9% of the data had negative x-intercept, indicating a negative diffusion coefficient, clearly an unphysical result. Negative intercepts were especially common when the upstream pressure increase was slow and the sample permeance was high (high P_m, small l), such that the time for the pressure to rise and the time to reach steady state are comparable. Negative intercepts also occurred in our previous study on PDMS.[12] Modification of the time lag equation in the manner suggested by Paul and Koros[23] does not correct this issue. With the proper theoretical treatment, it should be possible to correct the time lag equation for a non-step function increase in upstream pressure, but such a treatment is beyond the scope of the current work.

Table 3. Solubility parameters for the dual mode model from Reference [41].

		N_2	CO_2
S_d	mol/(L atm)	5.28×10^{-3}	4.18×10^{-2}
S_L	mol/L	3.13×10^{-4}	1.21×10^{-3}
b_L	1/atm	0.040	0.25

2. Molecular Dynamics

One value that is essential to the multiscale model but unknown experimentally is the sticking coefficient, which describes the probability of a gas molecule impinging on the polymer surface sticking for long enough to eventually be absorbed into the bulk polymer. To obtain this value, we performed MD simulations of CO_2 colliding with PPO. An entangled polymer structure consisting of 10 chains with 100 monomers per chain (17020 atoms) was created using the scaled effective solvent (SES) method[47] with cell dimensions of 58.9 x 58.9 x 58.9 Å. To create a PPO surface, a surface-cutting procedure was performed using the LAMMPS simulation package.[48] The length of the cell was increased by 200 Å in the z-direction to generate a region of empty space. All polymer chains were kept intact. A virtual Lennard-Jones wall was used to compact the dangling polymer chains at the surface to produce a final thickness of 5.89 nm. The surface was then equilibrated for 3000 ps in the NVT ensemble using the Berendsen thermostat at 300 K with a damping constant of 0.1 ps. The OPLS-2005 force field was used throughout.[49] The instantaneous surface was designated using the Gaussian smoothing method of Willard and Chandler.[50] The final, equilibrated structure has a density of 1.01 g/cm^3 and is shown in Figure 1.

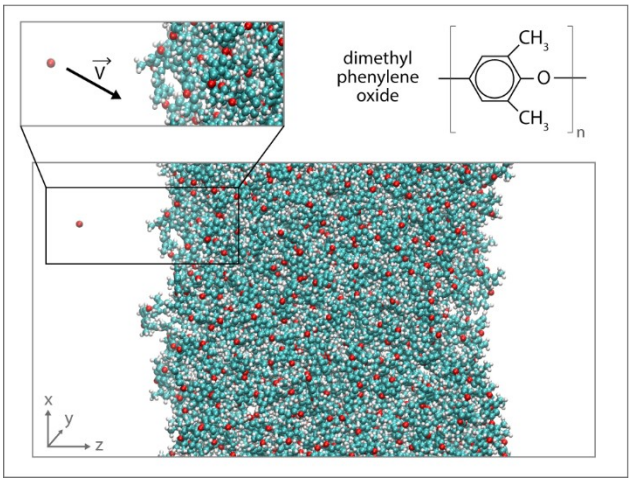

Figure 1. Polymer structure predicted from the molecular dynamics simulations, where blue represents carbon atoms, white is hydrogen, and red is oxygen. The molecule in the gas phase is CO_2, which is sent towards the surface with a velocity $\vec{v}$. The monomer 2,6-dimethyl-1,4-phenylene oxide chemical structure is shown on upper right.

A series of 265 simulations of CO_2 impacts onto the PPO surface was performed using the method from Julin *et al.*'s studies on the molecular adsorption.[51-52] A CO_2 molecule was placed approximately 15 Å from the PPO surface and was sent toward the surface (z-component of the velocity within a 45-degree cone) with a speed chosen randomly from the Maxwell-Boltzmann distribution at 300 K. The surface region of PPO was defined as ±4 Å of the instantaneous surface as defined by Willard and Chandler.[50] The position of the CO_2 molecule after 100 ps of NVE simulation determines the outcome - desorption, adsorption, or absorption. The impact simulations were performed using the Desmond MD simulation package[53-55] with a time

step of 1.0 fs for short-range interactions and 3.0 fs for long-range interactions. The short-ranged Coulomb cutoff is 9 Å and long-ranged Coulomb interactions were computed using the Ewald summation. Further details of the MD simulations can be found in our previous publication.[12]

Additionally, the free energy of CO_2 and N_2 within the polymer was determined using molecular metadynamics simulations. Five gas molecules were inserted into the simulation box, to produce a gas pressure of 2 atm; when all 5 gas molecules are sorbed into the polymer, this produces a concentration of 0.0404 mol/L. To estimate the free energy, one of the gas molecules was biased to encourage it to explore all possible energetic states through the thickness of the membrane while the other 4 gas molecules were allowed to move freely through the gas phase and the polymer (i.e. remain non-biased). The positions of 4 non-biased gas molecules were averaged over ~750 ns for the CO_2-PPO system and 600 ns for the N_2-PPO system to produce a number density, which gives an indication of the most favorable position for those molecules within the polymer. The bias force was directed from the center of mass of 1 gas molecule to and the center of mass of the PPO slab, which was located approximately at the center of the box; a counteracting force was applied to the polymer center of mass to prevent drift. The bias force had a Gaussian width of 0.05 Å, an initial Gaussian amplitude of 1.5 kJ/mol, a bias factor of 6, and a deposition period of 1.0 ps. A virtual wall was placed on either side of the membrane at $z = \pm 5.2$ nm

with a force constant of 500 kJ/(mol nm^2) in order to keep the gas molecules near the membrane.

Calculations were performed with a time step of 1.0 fs in the NVT ensemble using a stochastic global thermostat[56] with a coupling constant of 0.5 ps. The Lennard-Jones cut-off radius was 1.0 nm, where, the interaction was smoothly shifted to 0 after 0.9 nm. Unlike-atom interactions were computed using the standard Lorentz-Berthelot combination rules. Periodic boundary conditions were applied to all three directions. The short-range columbic interaction was treated within a cut-off radius of 1.0 nm while PME algorithm[57] with a grid spacing of 0.16 nm was used to calculate the long-range electrostatic interactions. All simulations were performed using Gromacs-2016.4[58-59] and plumed-2.4.1.[60] The OH-bonds on the PPO end groups were constrained by P-LINCS algorithm[61] with an order of 4. Further details on the metadynamics simulations can be found in the SI Section 2.

3. Multi-Scale Simulations

3A. Inductive modeling approach

The permeation of small gaseous molecules through a PPO membrane was simulated using multiscale reaction-diffusion kinetic models for single mode and dual mode permeation. The approach in this style of modeling is to assume the simplest description possible, then add complexity only when necessary.[62] For this reason, we begin with the model framework from a study of permeation of gases through a rubbery polymer.[12] We then expand upon that model by including dynamic changes in volume and the pressure-

dependent diffusion coefficients extracted from experiment. The goal of this part of the study is to determine the simplest model based in fundamental physical-chemical processes that reproduces the time-dependent permeation data.

3B. Numerical Procedure

The reaction-diffusion scheme is solved using a stochastic method,[63-64] a type of kinetic Monte Carlo (kMC), implemented in the open access package Kinetiscope.[65] A detailed derivation of the basic simulation algorithm for homogeneous, non-diffusing systems is given in Ref. [64], and its extension to simulate fully coupled reaction-diffusion systems is presented in Ref [66]. Briefly, the reacting system is represented by a collection of particles, each of which represents one or more molecules. All possible events in the system are written as reaction (chemical or physical) or diffusion steps. The rates for each reaction step are calculated in particles/sec units based on the rate coefficient and current concentrations using their appropriate reaction orders. The rates for each diffusion step are calculated based on the local diffusion coefficient and the current concentration gradient, also in particles/sec. All rates are converted to probabilities on a scale of 0 to 1 by dividing each rate by the sum of all the rates. Events are selected among the probability-weighted events using a random number between 0 and 1, and the time step calculated using a second random number and the reciprocal of the sum of the rates. After the event occurs and the simulation moves forward in time, the concentrations and gradients are updated, and the

event selection cycle repeats. The simulation terminates when the probability of all events falls to zero or a pre-specified time limit is reached.

The stochastic method is a rigorous solution to the master equation for Markov systems and produces an absolute time base when physically meaningful rate coefficients are used, in contrast to other kMC methods that only produce a relative time base. In addition, the stochastic method has advantages over continuum methods since it provides for simulation of complex systems in which swelling and other dynamic changes to the reacting environment occur, and for which detail at both nano- and macroscale dimensions is needed.

Model Development

The reaction-diffusion models are set up to allow for direct comparison of simulation predictions to experimental data on downstream pressure rise, as in our previous work.[12] A general schematic of the reaction-diffusion system is shown in Figure 2.

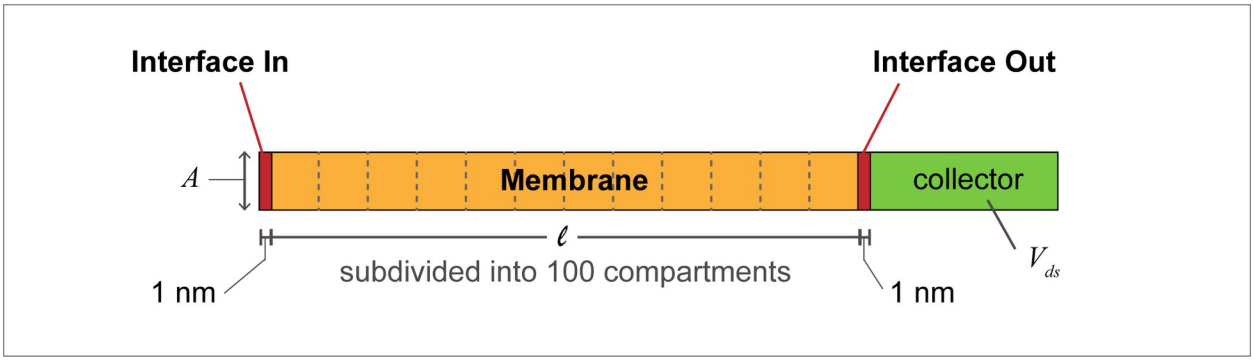

Figure 2. Schematic of the multiscale reaction-diffusion system equivalent to the membrane permeation system. The geometry, l, A, and V_{ds}, for each sample is taken from the experimental setup in Table 2. The collector is subdivided into 10 compartments with thicknesses increasing with distance from the Interface Out plane. Adjacent compartments are connected by a diffusion pathway for the gas.

1. Geometry

The cross-sectional area, A, upstream pressure, p_{up}, downstream volume, V_{ds}, and initial membrane thickness, l, are set to experimental values (see Table 2). The system is divided into a 1-dimensional array of smaller compartments. The interfaces of the polymer with the gas phase are assumed to be 1 nm thick on both sides of the membrane. The membrane bulk is sub-divided into 100 compartments of equal thickness. The gas collector with V_{ds} = 41.73 cm^3 is divided into 10 compartments with gradually increasing thickness starting from 10 nm and increasing in the direction away from the downstream interface. This construct minimizes the number of compartments required, and thus the cost of the simulation, while preventing artificially high concentration gradients (and therefore fast diffusion rates) that would have resulted if a large-volume collector compartment were placed next to the thin interface compartment.

2. Interfaces

The adsorption and desorption physical reactions are shown in Scheme 1. During adsorption, a site on the surface of the polymer, σ, accommodates

a gas molecule, which is denoted as gas(p), i.e. gas in the polymer phase. Desorption is the reverse of this process.

Interface Reactions

1A	Adsorption	$\sigma \longrightarrow$ gas(p)	$r = -\lambda k_{ads} [\sigma]$
1B	Desorption	gas(p) $\longrightarrow \sigma$ + gas(g)	$r = -k_{des} [\text{gas(p)}]$

Scheme 1. Reactions occurring in the interfacial compartments with their associated rate laws. Adsorption takes place at Interface In, and desorption at Interface Out. The reactant σ indicates a site on the surface of the polymer. Reaction 1A is pseudo-first order in site concentration because the upstream gas density is incorporated into k_{ads} (Equation 7).

The rate coefficient for interfacial adsorption, k_{ads}, is calculated from gas kinetic theory for the collision frequency, Z, of a gas at a pressure p_{up} with a planar surface at T = 308 K times the sticking probability, μ, determined from the molecular dynamics simulations.

$$k_{ads} = \mu Z A \lambda = \mu \left(\frac{p_{up}^{max}}{\sqrt{2\pi m k_B T}} \right) A \lambda \qquad (7)$$

where m is the molecular mass of the gas, A is the surface area, and k_B is Boltzmann's constant. The concentration of gas upstream is not included

explicitly in the rate equation for Reaction 1A because it is already included in the k_{ads} via p_{up}. Because the upstream pressure does not instantly reach its steady state value, the variable λ scales k_{ads} with the rise in upstream pressure:

$$\lambda = \frac{p_{up}(t)}{p_{up}^{max}} \quad (8)$$

where $p_{up}(t)$ is the upstream pressure at time t, and p_{up}^{max} is the maximum upstream pressure with which steady state properties are calculated.

During desorption, the gas in polymer moves to the gas phase in the collector, denoted as gas(g), leaving behind an available surface site σ that can be occupied by a new gas molecule emerging from the polymer bulk. The desorption rate coefficient, k_{des} = 1.4 × 10^{11} s^{-1}, is calculated from the Arrhenius equation using an activation energy for the breaking of a single van der Waals bond in the gas phase, and the pre-exponential factor is assumed to be 10^{13}.[67-68]

The concentration of surface sites is 1.66 mol/L, which is equal to a liquid surface site density of 10^{14} atoms/cm^2,[69] distributed through the 1-nm thickness of the interface. Our previous study[12] showed that the simulations are insensitive to the surface site concentration so long as it is greater than or equal to the bulk sorbed gas concentration.

3. Boundary Conditions and Diffusion Coefficients

Because we use a stochastic method, our boundary conditions (BC) are implemented differently than in coupled differential equation (CDE) solvers. Each compartment is connected to the adjacent compartments via Fickian

case I diffusion pathways for the sorbed gas molecules. Effects such as swelling and polymer relaxation that would result in non-Fickian diffusion are included explicitly as separate processes, and not integrated with the diffusion coefficient (more details are provided below). The connection of compartments by diffusion paths is analogous to flux (Neumann) BC in CDE, with the flux dependent on the local, time-dependent concentrations. The center-to-center distance between adjacent compartments is used for the calculation of concentration gradients.

The diffusion coefficients for gases within the membrane are calculated as described in Methods Section 2. Gases that have desorbed from the membrane move into and within the downstream collector volume with $D(\text{gas(g)}) = 7.43 \times 10^{-4}$ m^2/s, consistent with the mean free path and average velocity of CO_2 in the gas phase.[70] Gas molecules only contribute to p_{ds} once they are in the collector region, away from the membrane interface. Additional details for the gas collector compartments are available in the SI Section 3.

4. Initial Conditions and Pressure-Dependent Concentration of Permeants

The simulation start time is set to the beginning of the rise in upstream pressure, p_{up}, in the experiment, and the experimentally recorded $p_{up}(t)$ is used as an input. In literature models, the concentration at the interface and the solubility within the polymer are assumed to instantly equilibrate with the external pressure, and these conditions are imposed via thermodynamic equations (Eqn. 6). In our model, the increase in concentration at the

interface and in the polymer bulk are included in the form of physical conversion processes.

Within each compartment in the bulk of the polymer, we use computational constructs that are represented in Scheme 2. We use Ψ to denote a polymeric matrix that can accommodate a certain concentration of sorbed gas. The simplest implementation is in the single mode model (Reaction 2A), in which the polymer that is initially under vacuum, Ψ_v, is converted to a gas-exposed polymer, Ψ_p. The maximum concentration of gas(p) sorbed within Ψ_p is determined by the final upstream pressure and the gas solubility, and is calculated using Equation 1 or 2. The physical nature of gas accommodation does not need to be defined within this model, only the maximum sorbed gas concentration. Ψ_p (and therefore sorbed gas) is uniformly distributed within each compartment. The rate coefficient for this conversion process, k_{rise}, is set so that the time for Reaction 2A to be completed is equal to the time for the pressure to rise, as done in a previous study.[12] The values of k_{rise} are determined independently for each experimental run due to variations in the pressure rise profile from run to run; however, the same value of k_{rise} is used for each simulation of the same experimental run (i.e., without swelling, with swelling, and concentration-dependent diffusion). The rate law is zeroth order in polymer concentration, and tracks only the pressure rise; any information on interactions between the gas and polymer are contained within k_{rise}.

Change of Polymer from Vacuum to Pressurized Conditions

Single Mode Model

2A $\Psi_v \longrightarrow \Psi_p$ $r = -\lambda k_{rise}$

Dual Mode Model

2B $\Psi_v \longrightarrow \Psi^D_p$ $r = -\lambda k^D_{rise}$

2C $\Psi_v \longrightarrow \Psi^L_p$ $r = -\lambda k^L_{rise}$

Scheme 2. General scheme for the process by which the bulk polymer adjusts to the change in upstream pressure with their associated rate laws. The step for the single mode model (2A) is split into two separate steps (2B and 2C) for the dual mode model.

This description is generalized for the dual mode model by dividing Ψ_p between the dissolved mode, Ψ^D_p, and the Langmuir mode, Ψ^L_p, as shown in steps 2B and 2C, with the solubility within each mode calculated using the dual mode sorption parameters reported by Toi *et al*.[41]

5. Single-Mode Model

The single mode model treats all Ψ_p within the polymer as equivalent, similar to the treatment of permeation through rubbery polymers.[12] The diffusion coefficients for movement of solutes between compartments are calculated from the measured steady-state permeation data at each pressure using Equation 3.

5A. Swelling

Sorption of gases can lead to swelling, especially at high concentration. We account for the dynamic change in volume of each compartment, *i*, during the simulation by calculating the current volume at each time step, *V(t)*, using the equation

$$V(t) = \sum_i \frac{n_i(t)}{\rho_i} \quad (9)$$

where $n_i(t)$ is the amount of each substance at time t, and ρ_i is the molar density of that substance. We assume that all species are incompressible and that their occupied volumes are additive. The molar density ρ of the polymer is calculated by dividing the mass density of the polymer by the molar mass of its monomer, m = 120 g/mol in the case of PPO. This results in ρ = 8.83 mol/L. The partial molar volume, V_p, of CO_2 in a glassy polymer increases from 10 cm^3/mol in dilute form, and approaches 46 cm^3/mol (the same as CO_2 in organic solvents) at high concentration.[71] For this study, the limiting cases of no swelling and maximum swelling (V_p = 46 cm^3/mol) are tested.

More information on the effects of swelling is provided in SI Section 4.

5B. Concentration-Dependent Diffusion

Although the basic simulation assumes a constant diffusion coefficient, it is possible that the diffusion coefficient early in the experiment, when the polymer has been exposed to only a small concentration of gas, is different from the apparent diffusion coefficient at steady state when the internal gas concentration is at its maximum. Such a scenario would imply a change in polymer morphology, leading to Case II or anomalous diffusion at non-steady

state; at steady state, the experimental downstream pressure versus time data have a constant slope, indicating that any changes within the polymer have stabilized at that point. A computational scenario in which the diffusion coefficient changes due to gas exposure has been tested in this work using the method previously developed in Ref. [11]. The implementation is described in Scheme 3, where the polymer converts from an initial form Ψ_p to a subsequent form Ψ_F as the sorbed gas concentration increases using a second order reaction step. The rate constant $k_{D(c)} = 6 \times 10^8$ M^{-1} s^{-1} is calculated by assuming a diffusion-controlled interaction between gas molecule and a 1,3-dimethyl benzene monomer, as described in SI Section 3. The presence of the 2 forms, Ψ_p and Ψ_F, creates two diffusion environments that are treated as independent, parallel diffusion paths. Their relative importance changes dynamically as the sorbed gas concentration increases. Gas diffuses through the Ψ_p form with a diffusion coefficient that is equal to the y-intercept in a linear fit to the experimental diffusion versus pressure data (equation given in Figure 3), i.e. when the gas concentration is near zero. The diffusion coefficient for gas through the Ψ_F form is the apparent diffusion coefficient at steady state, $D_{app}(p_{up})$, given in Figure 3. It is possible that the conversion from Ψ_p to Ψ_F is slow, i.e., reaction-controlled rather than gas-diffusion controlled. This possibility was tested by reducing $k_{D(c)}$ over several orders of magnitude (shown in SI Section 5), but those permeation curves do not match the experimental data.

Concentration-Dependent Diffusion

3A $\Psi_p + \text{gas(p)} \longrightarrow \Psi_F + \text{gas(p)}$ $\quad r = - k_{D(c)} [\Psi_p] [\text{gas(p)}]$

Scheme 3. Reaction that alters the diffusion coefficient for the gases.

6. Dual-Mode Model

The dual mode model treats the sorbed gas within the polymer as two different populations, dissolved and Langmuir. It is unknown whether the same sorption mechanism governs dissolved and Langmuir populations, and so three different scenarios are tested by adjusting k^D_{rise} and k^L_{rise} in Reactions 2B and 2C:

(i) Langmuir sorption is set to its maximum value from the start of the simulation, dissolved sorption increases with the pressure rise (Ψ^L_p is present from the start, and Reaction 2C is omitted).

(ii) Both dissolved and Langmuir sorption increase simultaneously ($k^D_{rise} = k^L_{rise}$).

(iii) Dissolved and Langmuir sorption increase on different timescales ($k^D_{rise} \neq k^L_{rise}$).

Scenario (i) is most consistent with a strict interpretation of the dual mode model, where the void spaces for Langmuir sorption are an inherent part of the material structure, similar to zeolites. The other two scenarios include the possibility that the interactions between polymer and gas affect the

polymer structure and dynamics. In Scenario (ii), the two sorption modes respond similarly to gas absorption, whereas in Scenario (iii), they respond differently. The values of k^D_{rise} and k^L_{rise} are determined as fitting parameters that produce the correct downstream pressure versus time curves.

Typically, it is assumed that there is continuous, diffusion-controlled interchange of solutes between the two sorption modes. The rate coefficient for exchange between site types, $k_{exchange}$, was calculated from the Smoluchowski equation for a diffusion-controlled reaction, as detailed in the SI Section 3, resulting in $k_{exchange} = 2 \times 10^7$ M^{-1} s^{-1}. However, using this value produces an inefficient simulation where most of the computation time was being spent shuffling molecules between dissolved and Langmuir sites, a drawback of the simulation method. Therefore, for computational efficiency, we allow $k_{exchange}$ to be a much smaller value, 10^2 M^{-1} s^{-1}. The impact of this assumption was tested by running some of the simulations with $k_{exchange} = 10^3$ M^{-1} s^{-1} and $k_{exchange} = 10^4$ M^{-1} s^{-1}, and the results were identical (shown in SI Section 6). The insensitivity of the simulations to $k_{exchange}$ indicates that the exchange process is not kinetically controlling.

Exchange Between Sorbed Gas Populations

4A $\text{gas(D)} + \Psi^{L}_{p} \longrightarrow \Psi^{D}_{p} + \text{gas(L)}$ $\quad r = - k_{exchange} [\text{gas(D)}] [\Psi^{L}_{p}]$

4B $\text{gas(L)} + \Psi^{D}_{p} \longrightarrow \Psi^{L}_{p} + \text{gas(D)}$ $\quad r = - k_{exchange} [\text{gas(L)}] [\Psi^{D}_{p}]$

Scheme 4. Reactions for the exchange of gases between the dissolved (Ψ_p^D) and Langmuir (Ψ_p^L) sorption modes.

Results

1. Experiment

1A. PPO Membrane Properties

The density of the PPO membranes is measured to be 1.06 ± 0.09 g/cm^3, which gives a FFV of 0.190.[42-43] The Tg is 214 ± 7ºC. Compared to literature data, our samples have a lower density and a Tg in the middle of the range reported.[20, 41, 43, 46, 72-80] The large deviation in Tg is due to the broad peak in the DSC scans. The crystallinity is calculated to be 20.6%; reports of PPO crystallinity in the literature are rare, and the few reported values vary widely from 3% to 48%.[73, 79]

1B. Permeation Measurements

Sorption and permeability data are presented in Figure 3. The permeability coefficients, P_m, are calculated for each run from Equation 4 for upstream pressures, p_{up}, ranging from 1-18 atm, and are plotted in Figure 3b. The raw data for downstream pressure versus time from which P_m are calculated are presented in the SI Section 7, Figures S8 - S9. Changes in downstream pressure due to gas leaks, $(dp_{ds}/dt)_{leak}$, are less than 5% in all cases. The permeability coefficients for N_2 are consistent with previous reports from Toi *et al*.[41] The permeability coefficients for CO_2 in this study are

slightly greater than other values reported in the literature (see SI Section 1).[20, 24, 41, 46, 72, 79] Our analysis of data from Wright and Paul[46] shows that permeability decreases with increasing density, but has a non-monotonic relation to Tg (details in SI Section 8). Because our samples have a low density, though still within the range reported in other studies, it is to be expected that they will have a higher permeability. Both solubility and diffusivity of CO_2 in PPO are higher than N_2, even though CO_2 is the larger molecule.

1C. Diffusion Coefficient Determinations

The measured steady state permeation data are fit with both the dual and single mode models to extract diffusion coefficients for the simulations. Results using the dual mode model for permeation (Eqn. 3 and Figures 3a and 3b) are listed in Table 4 and are used in the dual mode multiscale simulations. The standard deviation represents ±5.5% and ±4.7% from the non-linear dual mode fit for N_2 and CO_2, respectively. The assumption that there is a simple linear relation between P and p_{up} (shown in SI Section 9 Figure S11) results in no change to the standard deviation, indicating that the more complex non-linear fitting of the dual mode model may not be necessary. Recalculating the permeability coefficients using the final thickness predicted by simulations (i.e., accounting for swelling) changes their values by <5%.

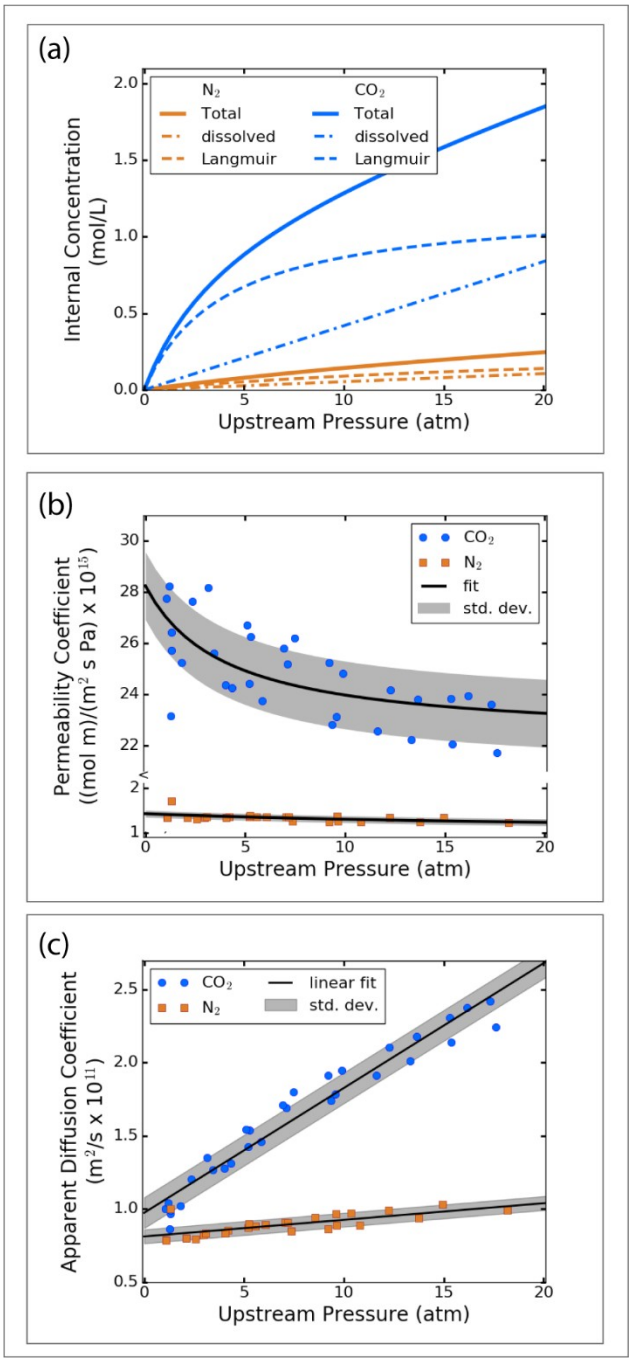

Figure 3. Isotherms as a function of upstream pressure. (a) Dual mode sorption, using the sorption isotherms from Ref. [41] The total sorbed gas concentration (solid lines) is divided into the dissolved mode (dot-dash lines) and the Langmuir mode (dashed lines). (b) Dual mode permeability values for N_2 (orange squares) and CO_2 (blue circles), shown for all PPO samples.

The black lines are a fit using with parameters listed in Tables 3 and 4. The gray area shows one standard deviation. (c) Single mode apparent diffusion coefficients calculated using data in (b).

Single mode apparent diffusion coefficients, D_{app}, were calculated using data in Figure 3b, Eqn 1, and S_d from Table 3. For both N_2 and CO_2, D_{app} increases with increasing pressure, indicating that the presence of gas changes the environment within the polymer to ease transport of additional gas. D_{app} vary linearly with p_{up}, with $D(CO_2)=(0.0853\,p_{up}+0.974)\times10^{-11}$ m^2/s, 11 % standard deviation, and $D(N_2)=(0.0114\,p_{up}+0.812)\times10^{-11}$ m^2/s, 5.9 % standard deviation.

Table 4. Diffusion coefficients for N_2 and CO_2 in PPO, by fitting the experimental permeability data with the dual mode permeation model (Eqn 6).

	D_d	D_L
	m^2/s	m^2/s
N_2	1.886 × 10^{-11}	3.528 × 10^{-12}
CO_2	5.391 × 10^{-11}	2.003 × 10^{-12}

2. Molecular Dynamics

The density of the polymer in the MD simulations is 1.01 g/cm^3, which is lower than the 1.06 g/cm^3 in the experiment. This discrepancy is most

likely due to the short chain lengths (100 monomers) and the small thickness (< 6 nm) used for the MD study. Currently, it is necessary to simulate small systems due to the computationally intensive nature of MD. Because of these limitations, we use the results of the MD studies in a limited manner.

2A. Interfacial Sticking Probabilities

The sticking coefficient refers to a kinetic factor, the probability of a gas impinging on a surface to remain on the surface. It is distinct from the solubility or uptake, which is the probability for a molecule in the gas phase to move into the bulk region of the polymer.[81] Results of the molecular dynamics simulations to determine a sticking coefficient for CO_2 on PPO are shown in Figure 4. Trajectories are classified as representing adsorption, desorption and absorption events based on the position of the CO_2 molecule at the end of 100 ps. Some care must be taken in how the classification of type of event is interpreted: the distinction between an adsorbed and absorbed molecule is arbitrary, especially for atoms just below the gas-polymer interface, and the fate of molecules adsorbed on the surface is not clear from the finite simulation time. Thus, sticking in these simulations has a lower bound of 13%, equal to the fraction of absorbed molecules, and an upper bound of 40%, equal to the fraction of absorbed plus adsorbed molecules.

The minimum sticking coefficient of μ = 13% is used in the reaction-diffusion simulations for all gas molecules. This value is lower than our previous findings for CO_2 sticking to the surface of poly(dimethyl siloxane) (PDMS) of 30%[12] but is within the range of 10% to 100% found in other

systems studied by molecular dynamics (MD) at room temperature.[51-52, 82-84] Our previous study showed that the multiscale model is insensitive to the precise value of the sticking coefficient over a range of several orders of magnitude, and so any errors due to the low density or slight differences between CO_2 and N_2 will not affect the multiscale modeling results. The interaction that determines how well a gas molecule will stick to a polymer surface is not well understood, and the data collected in this study did not provide any additional insights beyond what has already been published.[51-52, 83-85]

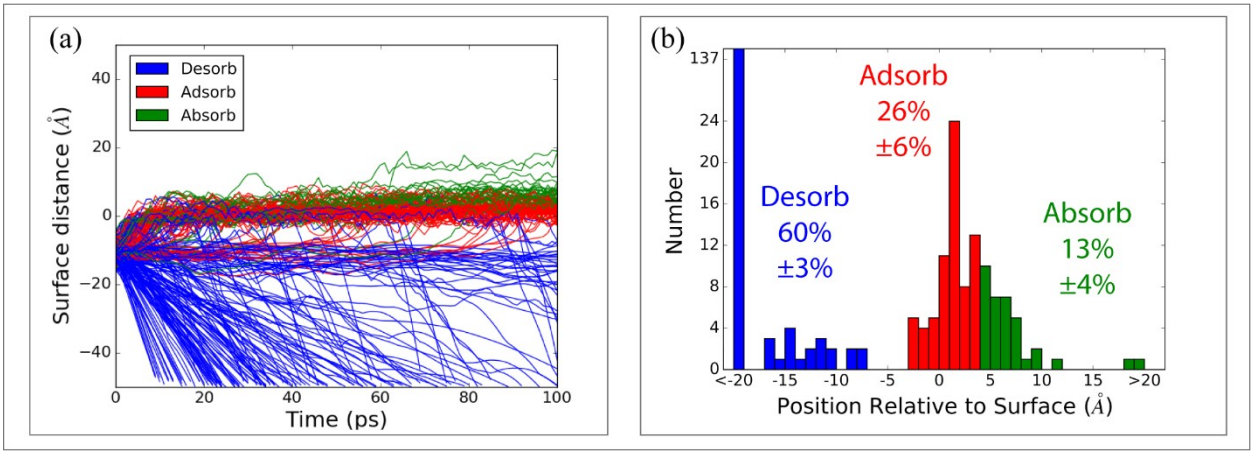

Figure 4. Results of the molecular dynamics simulations of CO_2 sticking to PPO. For both panels the surface is defined as position 0 with positive positions occupied by the polymer and negative positions corresponding to an empty region. (a) Distance from the instantaneous surface as a function of time for all 265 trajectories. (b) Histogram of outcomes from all CO_2 impacts onto the PPO surface.

2B. Free Energy Profile

The results of the free energy calculations are reported in Figure 5. In Figure 5a, both CO_2 and N_2 have a higher (less favorable) free energy in the gas phase. The variations in the gas phase free energy are due to interactions with other gas molecules and to long-ranged electrostatic and van der Waals interactions with the polymer. Both gases experience a decrease in free energy in the surface region of the polymer compared to the gas phase. The decrease in free energy is due to enthalpy, since entropy should decrease upon gas sorption into the polymer; additional studies at other temperatures would be required to determine the precise entropic contributions to the free energy change. N_2 appears to have a greater affinity for the surface region, whereas CO_2 finds the surface less favorable than the bulk, though for both gases, their most favorable position (minimum free energy of 0 kJ/mol) is located in the bulk. The difference in free energy between the gas phase and the bulk region gives the affinity of the gas for the polymer; CO_2 has a stronger affinity of ~18 kJ/mol compared to 7 kJ/mol for N_2. Qualitatively similar results are seen in the number density of gas molecules based on position shown in Figure 5b. The density profiles demonstrate that both CO_2 and N_2 have the same density at the surface. However, the greatest number of N_2 molecules, on average 2.2 out of 4 N_2 molecules, reside in the gas phase, implying that they favor a position near the PPO surface but not in contact with it. In contrast, a greater number of CO_2 molecules, on average 3.2 out of 4 CO_2 molecules, exist in the PPO bulk.

The free energy profile (Fig. 5a) for CO_2 in the PPO bulk features several ups (peaks) and downs (basins) with moderate energy barriers separating the states. Moderate energy barriers allow CO_2 to hop more frequently between the open spaces during polymer segmental motion. In contrast, N_2 has fewer peaks/basins but with high energy barriers, especially near the center of mass of the polymer, suggesting that the trapped N_2 molecules wait longer for a forward jump. The diffusion of N_2 and CO_2 is depicted in SI Section 10 in Figures S12 and S13, which confirm that CO_2 has larger displacements more frequently than N_2 and supports the idea that the higher diffusivity of CO_2 over N_2 can be attributed to its more frequent jumps within the polymer structure. Figures S12c-f and S13c-f show that CO_2 passes through the entire PPO slab 20 times in total but N_2 has only 1 successful pass, which suggests that CO_2 has 20 times greater permeability over N_2. This value is remarkably (and perhaps fortuitously) close to ratio of the experimental permeabilities of 19 at 2 atm. While the absolute values of free energy may shift if the polymer density were closer to the experimental value, the comparative behavior of N_2 and CO_2 should remain valid.

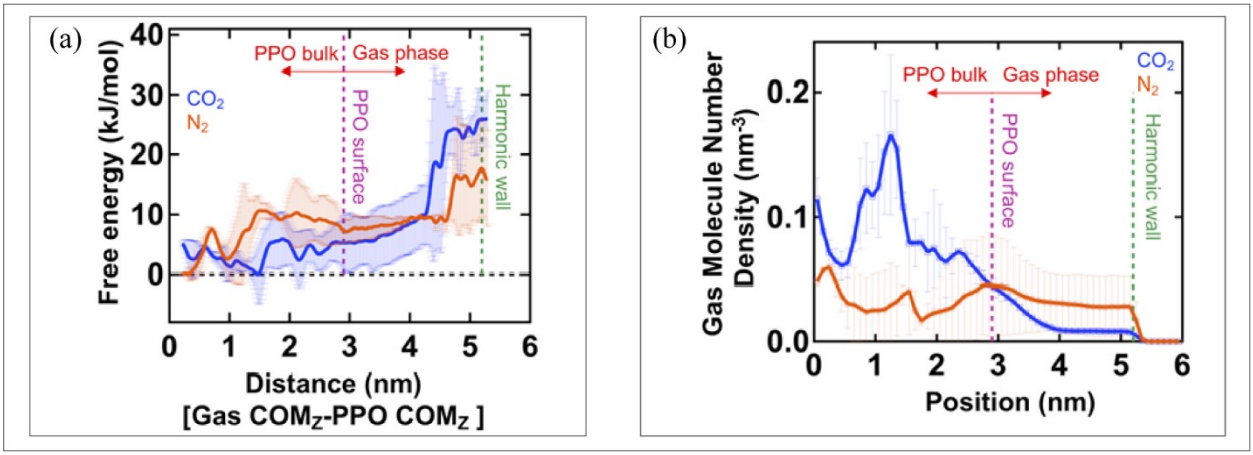

Figure 5. (a) Free energy profile of the biased N_2 (orange) and CO_2 (blue) molecule as a function of distance in the z-direction between the center of mass (COM) of the gas molecule and the COM of PPO. (b) Number density of the non-biased N_2 (orange) and CO_2 (blue) molecules with respect to position in the z-direction, which is normal to the surface of the polymer slab where 0 is the center of polymer. Both plots show the average and standard deviation between positive and negative z-positions. The surface position is defined as the point at which the PPO density falls to half of its bulk value, averaged between the CO_2 and N_2 systems. The surface width, as defined by the distance between the 10% and 90% density positions in the "10-90" Gibbs division surface definition is 1.3 and 1.4 nm for the CO_2-PPO and the N_2-PPO system, respectively.

3. Multi-Scale Reaction-Diffusion Simulations, Single Mode Model

The result of the simulations of PPO permeation by N_2 and CO_2 are presented as the downstream pressure versus time and compared to experiment in Figures 6-9 for the single mode model and its variations. The

results for a membrane thickness of 22.4 μm with $p_{up}(CO_2)$ = 1.82 atm and $p_{up}(N_2)$ = 7.38 atm are presented in the main text because they display the largest difference between rubbery and glassy behaviors. The input values used are listed in Table 5. Additional figures showing similar findings for other membrane thicknesses and gas pressures are provided in SI Section 11.

For N_2 (Fig. 6a, 7a, 8a, 9a), the upstream pressure rises in 3.13 s. If the polymer conversion process (Model Development section 4) is also completed in 3.13 s, indicating an instantaneous equilibration between upstream pressure and internal polymer state, then the simulated pre-steady state downstream pressure does not agree with experiment. Figure 6a compares such an instantaneous response to the response calculated when k_{rise} is treated as an adjustable (non-instantaneous) parameter that brings the simulation results for pre-steady state into agreement with the experiment. As seen in Table 5, the non-instantaneous value for k_{rise} is smaller than the instantaneous value, and the conversion reaction is slower. We estimate that completion of the polymer conversion reaction (Reaction 2A) for maximum gas uptake requires 24.0 s for N_2 under these specific experimental conditions. Similarly, for CO_2 (Fig. 6b. 7b, 8b, 9b), the upstream pressure rises over the course of 2.08 s, but the polymer conversion is completed at 17.4 s in the simulations that match experiment. This indicates that for both gases the equilibration of the polymer with the upstream gas pressure is delayed, in contrast to the standard assumption of instantaneous

equilibration and in contrast to the previously observed behavior in rubbery polymers.[12] The experimental apparatus is the same as that used in the rubbery polymer work,[12] so if the delay were due to instrumental artifacts, it would have been seen in the earlier work as well.

The values of k_{rise} for instantaneous and non-instantaneous equilibration for both gases were determined using the swelling single mode model, and then the same set was used for the constant volume and concentration-dependent diffusion coefficient simulations.

Table 5. Inputs for single mode simulations

		N_2	CO_2
Sample		2	2
p_{up}	atm	7.38	1.82
$[gas(g)]_{init}$	mol/L	5.20×10^{-7}	4.68×10^{-7}
$[gas(p)]_{max}$ in Ψ_p	mol/L	0.110	0.4554
k_{rise} (instantaneous)	M s^{-1}	0.1	0.5
k_{rise} (non-instantaneous)	M s^{-1}	0.007	0.035
D_{app}	m^2/s	8.494×10^{-12}	1.023×10^{-11}

3A. Single Mode Model with Constant Volume

Permeation curves for the single mode model without swelling are shown in Figure 6. The assumption of instantaneous equilibration leads to

809 erroneous pre-steady state behavior, whereas non-instantaneous
810 equilibration matches experiment at both pre-steady and steady state.
811

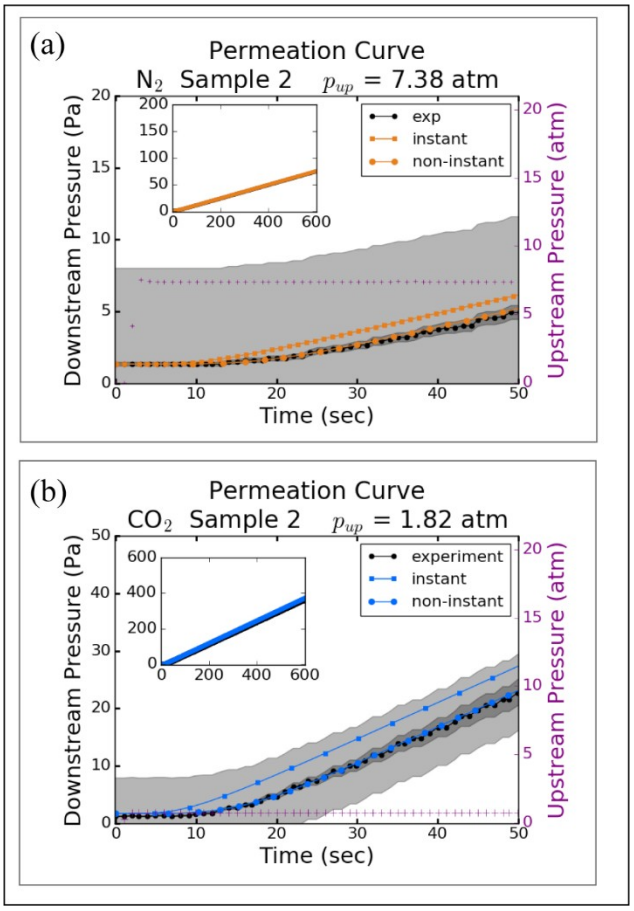

812

813 **Figure 6**. Permeation curves for the single mode model without swelling for
814 (a) N_2 and (b) CO_2 using instantaneous (squares) and non-instantaneous
815 (circles) equilibration between the external pressure and bulk polymer state.
816 The gray region represents a measurement error of approximately 10%.
817 Note that the axes' scales are different for N_2 and CO_2 so that the details in
818 both sets of curves can be seen.
819

3B. Single Mode Model with Swelling

Permeation curves for the single mode model with the maximum amount of swelling are shown in Figure 7. Again, the assumption that equilibration between the bulk polymer and upstream pressure is instantaneous leads to incorrect pre-steady state behavior. Assuming a non-instantaneous response results in simulations that match experiment. The effect of swelling on the permeation kinetics is negligible.

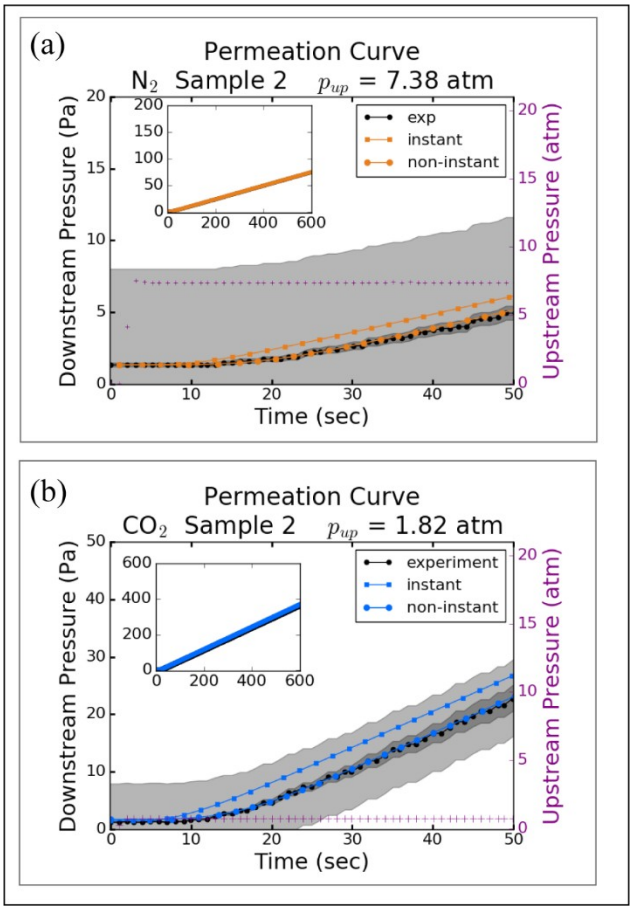

Figure 7. Permeation curves for the single mode model with the maximum amount of swelling for (a) N_2 and (b) CO_2 using instantaneous (squares) and non-instantaneous (circles) equilibration between the external pressure and

bulk polymer state. The gray region represents a measurement error of approximately 10%. Note that the axes' scales are different for N_2 and CO_2 so that the details in both sets of curves can be seen.

3C. Single Mode Model with Concentration-Dependent Diffusion

We tested the possibility that the steady-state pressure-dependent diffusion coefficients shown in Figure 3c are incorrect during the pre-steady-state regime, i.e. are dependent on local gas concentration in the polymer during the pressure rise. This is an alternative explanation for the discrepancy between instantaneous response predictions and experimental observations. Simulation results using the method and diffusion coefficients described in Model Development Section 5b and SI Section 5 for the single mode model with swelling are shown in Figure 8. It is evident that even with concentration-dependent diffusion coefficients, assumption of a non-instantaneous equilibration of the bulk polymer to the upstream pressure increase is necessary to match experiment. These results show that swelling and concentration-dependent diffusion do not account for pre-steady-state permeation behavior.

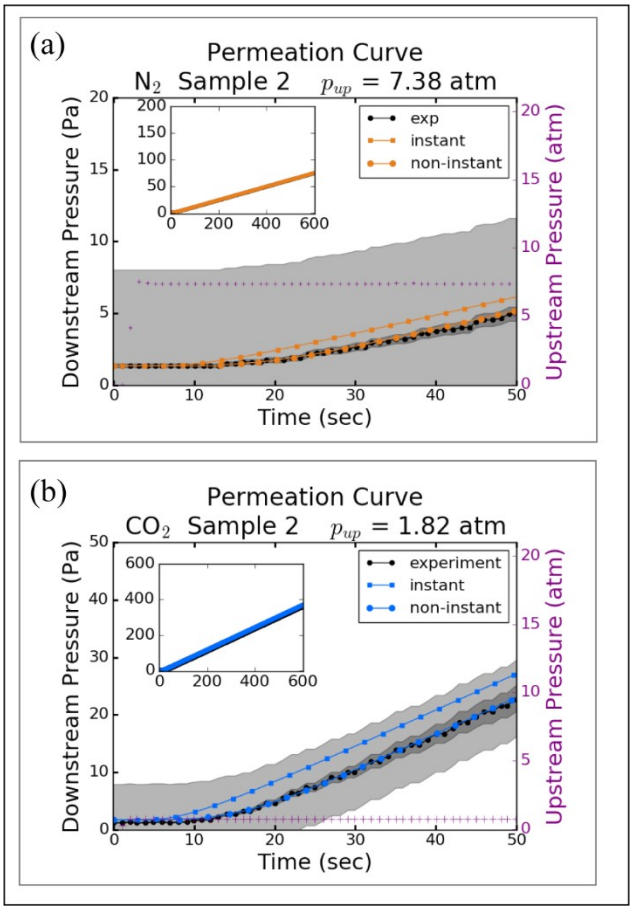

Figure 8. Permeation curves for the single mode model with swelling and gas concentration-dependent diffusion for (a) N_2 and (b) CO_2 using instantaneous (squares) and non-instantaneous (circles) equilibration between the external pressure and bulk polymer state. The gray region represents a measurement error of approximately 10%. Note that the axes' scales are different for N_2 and CO_2 so that the details in both sets of curves can be seen.

3D. Delayed Polymer Response in the Single Mode Model

Non-instantaneous equilibration between the bulk polymer and the external pressure during pre-steady state gas permeation has not been

previously reported. In order to rule out any potential artifacts from our simulation methodology, deterministic multi-physics simulations using COMSOL[86] were performed to predict the permeation curves (Fig. 9). Both deterministic and stochastic simulations predict incorrect pre-steady state behavior if instantaneous equilibration is assumed.

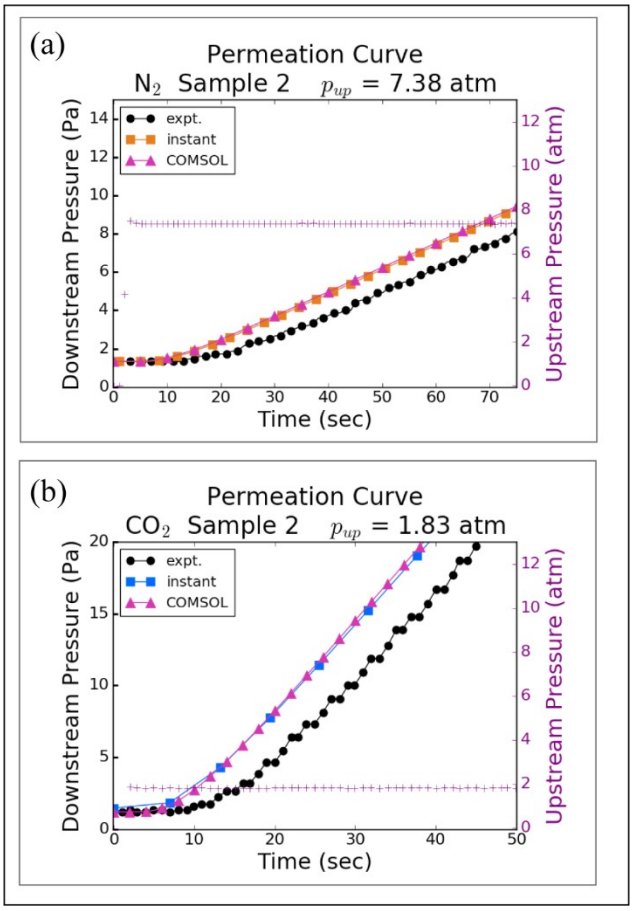

Figure 9. Comparison of permeation curves for (a) N_2 and (b) CO_2 from different modeling approaches. The results from COMSOL match the (Kinetiscope) model with instantaneous equilibration and no swelling. Note that the axes' scales are different for N_2 and CO_2 so that the details in both sets of curves can be seen.

Figures S14 - S16 in SI Section 11 present simulation results in comparison to experiment for a full range of upstream gas pressures. k_{rise} was determined independently for each experimental run, values are presented in Table S2.

Using these results, we calculated the percent difference in the timescales to reach the maximum solute concentration within the polymer and to reach the maximum upstream pressure. A percent difference of zero at all times would correspond to instantaneous equilibration. What is found is that the percent difference is very large when the pressure rise time is short, and decreases exponentially with increasing pressure rise time for both gases, as shown in Figure 10. The behavior in Figure 10 is consistent with ideas from linear response theory (LRT),[87] if we consider the polymer to be in a pseudo-equilibrium state before the gas is introduced in the experiment, and after the gas pressure reaches steady state. LRT says that when the state of a system strongly driven, such as with a rapid change in pressure, the system will take some time to relax to its new equilibrium state. In contrast, a weakly driven system, such as with a slow pressure rise, can be considered as a pseudo-equilibrium system throughout the course of the state change. The results in Figure 10, when combined with the data in Figure 3c showing that the pressure-dependence of the diffusion coefficients for N_2 is much weaker than for CO_2, point to the relaxation time as being characteristic of the PPO-gas combination. It should be noted that this relaxation occurs even when the solute is inert to the polymer (N_2),

suggesting that the mere presence of the solute affects polymer structure. Although it appears from Figure 10 that the polymer response could possibly be somewhat slower in the presence of N_2, the scatter in the data is too large to make this claim.

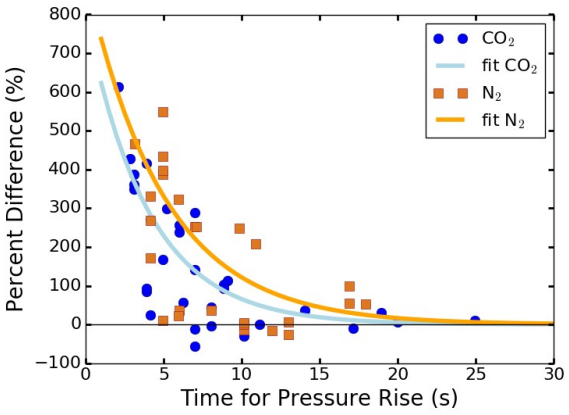

Figure 10. Percent difference between the time for the increase in pressure-dependent maximum concentration in the polymer and the upstream pressure rise time for CO_2 (blue circles) and N_2 (orange squares) as a function of upstream pressure rise time. The solid lines are an exponential decay fit to the data where $y(CO_2)=800e^{-0.25x}$ and $y(N_2)=900e^{-0.20x}$.

Throughout this work, the rate coefficient, k_{rise}, is used as an adjustable parameter and does not correspond to a primary process. We can hypothesize that k_{rise} contains contributions from the rate of pressure increase, the final pressure, polymer response, *etc*. To investigate the physical mechanism and determine a series of elementary steps for the

polymer conversion process, we would need to develop new instrumentation to record detailed information on the dose-response timings in this system and on sample-to-sample variations, accompanied by in situ modulus measurements. We suggest that new experimental work of this type would be invaluable for gaining new insights to gas-polymer interactions. The multiscale model framework described here can be readily extended to include additional details, and would help develop a robust connection between permeation theory and data. This would allow apparent, pressure-dependent diffusion coefficients to be directly and quantitatively linked to polymer relaxation processes.

4. Multi-Scale Reaction-Diffusion Simulations, Dual Mode Model

In the dual mode model, the sorbed gas is split into 2 populations, gas(D) and gas(L), which are associated with Ψ_p^D and Ψ_p^L, respectively. As in the single mode model, neither the precise nature of the polymer matrix nor the physical nature of gas accommodation need to be specified. The gas associated with each mode is treated as being distributed evenly throughout the compartment.

Three possible scenarios for how the polymer matrix adjusts to the pressure rise are tested, as described in Model Development Section 6. The input variables for the dual mode simulations of N_2 at 18.18 atm and CO_2 at 17.23 atm are listed in Table 6, and the associated values for k_{rise}^D and k_{rise}^L are listed in Table 7. As shown in Figure 11, each of the scenarios can

properly describe the pre-steady state downstream pressure increase. The results of additional dual mode simulations are shown in SI Section 12, together with the corresponding input variables.

The contribution of the dissolved and Langmuir modes to transport depends on the concentration gradient of sorbed gas within their respective populations multiplied by their characteristic diffusion coefficient. In all cases, the dissolved mode diffusion coefficient, D_d, is much larger than the Langmuir diffusion coefficient, D_L (see Table 4). Therefore, when the solute concentration profile of each type in the polymer is similar, most of the flux occurs via the dissolved mode due to its higher diffusion coefficient. On the other hand, when the Langmuir-type concentration is much larger than the dissolved concentration, like at low pressures (see Fig. 3a), most of the permeation flux is by the Langmuir mode due to its higher concentration gradient.

Table 6. Values of input variables for the dual mode simulations.

		N_2	CO_2
Sample		4	3
p_{up}	atm	18.18	17.23
$[gas(g)]_{init}$	mol/L	3.64 × 10-7	4.16×10^{-7}
$[gas(p)]_{max}$ in ψ_p^D	mol/L	0.0960	0.725
$[gas(p)]_{max}$ in ψ_p^L	mol/L	0.132	0.984

Table 7. Values of k^D_{rise} and k^L_{rise} for Scenarios (i) - (iii) of the dual mode model for the sample number and upstream pressure shown in Figure 11.

Scenario	N_2		CO_2	
	k^D_{rise}	k^L_{rise}	k^D_{rise}	k^L_{rise}
	M s^{-1}	M s^{-1}	M s^{-1}	M s^{-1}
(i)	0.003	n/a	0.06	n/a
(ii)	0.004	0.004	0.08	0.08
(iii)	0.003	0.1	0.06	0.1

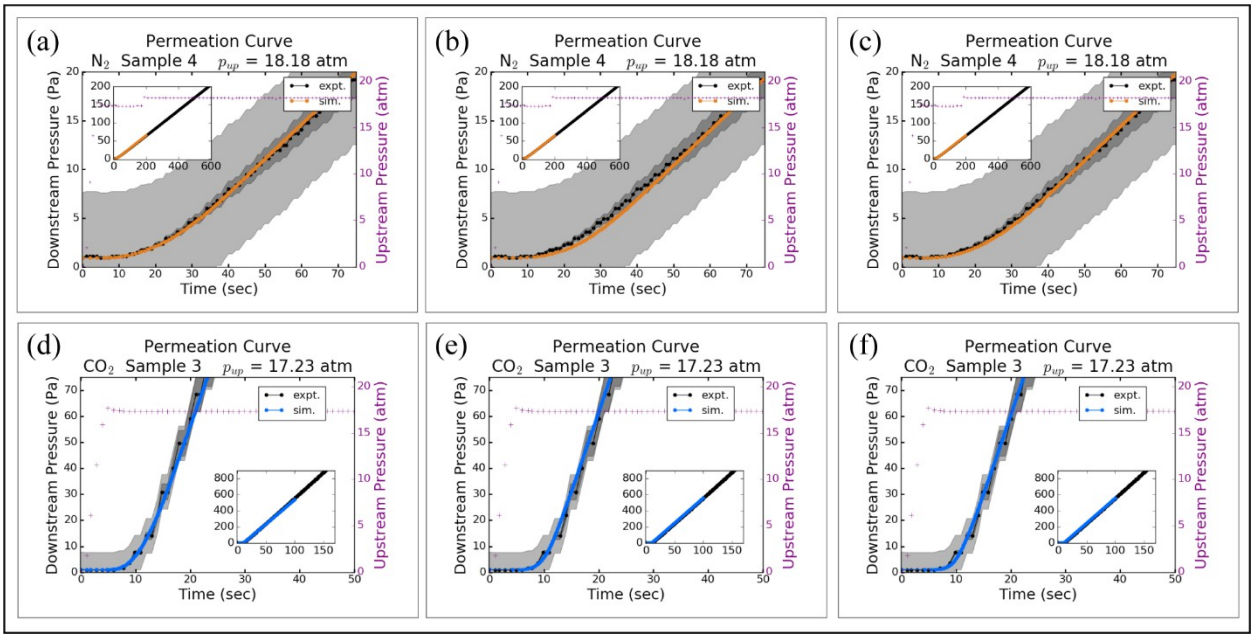

Figure 11. Permeation curves for (a-c) N_2 (orange) and (d-f) CO_2 (blue) with three different descriptions of the increase in maximum permeant concentration in the polymer: (a,d) Scenario (i) in which Langmuir sorption can occur from the start of the simulation, but dissolved sorption is related to

964 the pressure rise. (b,e) Scenario (ii) in which both dissolved and Langmuir
965 sorption increase at the same time. (c,f) Scenario (iii) in which dissolved and
966 Langmuir sorption increase on different timescales. The gray region
967 represents a measurement error of approximately 10%. Note that the axes'
968 scales are different for N_2 and CO_2 so that the details in both sets of curves
969 can be seen.
970

971 ## Discussion

972 This work seeks to develop and validate a single computational
973 framework for simulation of permeation of gases through glassy polymers
974 under both non-steady-state and steady-state conditions. We have examined
975 two main permeation models for this framework - single and dual mode -
976 with several variations of each. By comparing simulations to experiments, we
977 find that the full time-dependent permeation behavior can only be accounted
978 for by incorporating non-instantaneous equilibration between external
979 pressure and the maximum solute uptake of the polymer into the framework.
980 Neither swelling nor concentration-dependent diffusion coefficients can
981 account for the observations. In addition, the simulation results indicate that
982 both the dual mode and single mode models can correctly reproduce
983 experimental data. Accordingly, the dual mode model has no advantages
984 over a single mode model for accurately capturing time-dependent
985 permeation, but has disadvantages in terms of added model complexity.
986 Minelli and Sarti have similarly shown the adequacy of a single transport

mode using the non-equilibrium lattice fluid model (NELF) model.[88-89] The present work adds to a growing body of work that calls into question a physical interpretation of the dual mode model.

In general, the values for solubility and diffusivity (S_d, S_L, b_L, D_d, D_L) in the dual mode model are found by a non-linear fit to Equations 2 and 3. The values of these parameters are non-unique, i.e., multiple sets of values can fit the experimental isotherms equally well (SI Section 1).[20, 24, 41] Moreover, the best-fit values also depend on the pressure range over which the isotherms are investigated, with an increase in S_L and decreases in S_d and b_L as the upper end of the range increases.[25] While these parameters can be correlated with a variety of physical properties of the polymer and gas (e.g., Tg, FFV, $\rho(\text{gas}_{(p)})$), the correlations are weak due to a large degree of scatter in the data, especially when comparing between different structural families (e.g., poly(phenylene oxides) vs polysulfones).[26] Typically, the dissolved mode diffusion coefficient is an order of magnitude faster than the Langmuir diffusion coefficient.[41, 90-93] While coefficient values could correspond to two different fluctuation modes of the polymer, there is no *a priori* reason to associate one parameter with the dissolved mode and the other with the Langmuir mode. Furthermore, the dual mode model treats transfer between dissolved and Langmuir sites as instantaneous, so it is unclear how each of these two modes could contribute uniquely to transport. Moreover, the diffusion coefficients are uncorrelated with the critical volume of the gaseous permeants. Therefore, it appears that the dual mode solubility and diffusivity

values should be treated simply as empirical fitting parameters and not literally indicating two additive modes of sorption and transport at the molecular level.

Experimentally, it is observed that the volume of polymers decreases more slowly with decreasing temperature below the glass transition temperature than above it.[14-15] The difference between the glassy volume and a hypothetical rubbery volume at that temperature is defined as the excess free volume. Using positron annihilation lifetime spectroscopy (PALS), the excess free volume is shown to appear as an increase in magnitude of both the FFV and the FVE size in pristine glassy polymers.[18] Although the dual mode model is not clearly connected to physical properties of the gas-polymer systems, it does raise the question of whether excess free volume in glasses contributes to permeation in a manner that is different from that for free volume in rubbers.

If glassy polymer permeation consists of filling pre-formed voids, analogous to the internal space in zeolites, then simple space-filling arguments should account for the majority of sorption. However, the amount of N_2 sorbed via the Langmuir mode in a dual-mode analysis is typically less than the amount of CO_2,[41, 90, 93] even though N_2 has the smaller critical volume. We use molecular dimensions in our analysis because they describe a fundamental molecular property, the space occupied by a molecule's electron cloud. Though the kinetic diameters are commonly used in the

polymer membrane community, those values are based on equilibrium sorption into zeolites,[94] a scenario that is not necessarily directly translatable to diffusion through polymers. Furthermore, the kinetic diameter is often thought of as a shape correction for oblong molecules, but this correction is not applied consistently. For example, both N_2O and CO have the same length-to-width ratio (see Table S6), but only one of them receives a shape correction in the original work of Breck.[94] While the kinetic diameter is convenient for placing CO_2 within the trends for *P* and *D* versus size of other light gases, based on the considerations described here, it should not viewed as a fundamental molecular property (see SI Section 13 for further discussion of this point).

Furthermore, PALS studies on polycarbonate[27] and polysulfone[28] show that the FFV and FVE size distribution are not inert properties of the polymer material but can increase with sorption of CO_2. So even though CO_2 is filling some void space, it is also inducing a polymer relaxation that creates additional void space. The additional void space may be created by an increase in spacing between polymer segments that has been observed with wide angle x-ray diffraction (WAXD) after CO_2 sorption into poly(methyl methacrylate) and polycarbonate.[33] In the same study,[33] N_2 was shown to decrease the spacing between polymer segments, which may be the reason for its lower diffusion coefficient. The amount of void space created in polysulfone by CO_2 decreases slowly (over 10 hours) during exposure to vacuum.[28] Though the diffusion coefficient is known to increase with an

increasing amount of FFV at steady state,[20] the role that the void spaces play during non-steady state permeation is not well understood. The results from our simulations of permeation with a reaction-diffusion representation of the dual mode model indicate that several hypotheses for the behavior of the void spaces during pre-steady state are reasonable, so long as the overall polymer response is delayed from the upstream pressure rise, as was also observed with the single mode model.

The nanoscopic features of sorption and diffusion in polymers can be investigated directly with MD. In MD for glassy polymers, gas molecules are observed to occupy both void spaces and sites in which the polymer chains form a full coordination shell; these two types of sites are typically assumed to correspond to the Langmuir and dissolved sites, respectively, in the macroscopic dual mode description.[95] The void spaces obey a Poisson distribution with a high probability of finding very small voids and reduced probability of finding increasingly larger voids.[38] This is in contrast to the distribution implicitly assumed in the dual mode model, in which all void spaces are identical.[38] MD simulations of gas sorption in which the polymer structure is held static predict sorption isotherms that resemble classical Langmuir sorption isotherms, but are inconsistent with those for glassy polymers.[38] Allowing polymer relaxation during sorption produces isotherms that are more consistent with experiment.[38, 96] This polymer relaxation in the presence of CO_2 is associated with shifting the FVE distribution to larger sizes.[38] It is unclear if the shift in FVE distribution is the same polymer

relaxation being invoked in this work; additional experimental data would be needed to prove this connection.

MD investigations of gas transport through glassy polymers shows that when gas molecules occupy a void site, they explore the full surface area of the void, and the rate-limiting step for their forward motion is polymer chain fluctuation creating a channel between voids then closing off space behind the molecule.[35-37] The same type of “jump” diffusion in which molecules hop between FVE is observed in rubbery polymers;[34] however, the channels in a glassy polymer are longer-lived, meaning that the gas must wait a longer time for a productive forward jump, though still only on the order of nanoseconds.[35-36] The free energy barriers for these jumps are shown to depend on the gas-polymer interactions (Fig. 5), resulting in different diffusion coefficients for different molecules even though polymer segmental motion is the rate-limiting step in both cases.

The permeation mechanism evaluated in the present study for N_2 and CO_2 through PPO over extended time scales is consistent with this nanoscopic physical picture. The pressure-dependence of the diffusion coefficients in Figure 3c reveals that anomalous diffusion, in which both penetrant concentration gradient and polymer environment play a role, is operant. The presence of sorbed gas causes a relaxation (Figure 10) whose response time is roughly independent of gas type and thus appears to be polymer-dependent. In addition, the pressure dependence of the

phenomenological diffusion coefficients in Figure 3c signals a change in the polymer structure with increasing permeant concentration. This effect is much more pronounced for CO_2 than for N_2. From consideration of the literature,[27-28, 33, 38] it is likely that this polymer relaxation is related to the creation of FFV, but the reported time scale for this process is too fast to be probed directly by our current set of studies. This suggests that slower processes may also be involved. It is unclear from this study if the difference in free energy barriers in Figure 5a is a result of changes in FFV, differences in intermolecular interaction energies, or a combination thereof. Our work adds weight to the argument that polymer relaxation governs transport in glassy polymers by showing that it is kinetically significant not only on the very short timescales accessed by MD, but is also a general feature of non-steady state permeation of PPO for both CO_2 and N_2. The present study also augments the physical picture presented by MD calculations by revealing the importance of a timescale for the overall polymer response of the order of a few seconds, and the significant influence of a changing polymer environment on the macroscopic diffusion coefficient.

Alternative models to the dual mode model are available but have not yet been widely adopted in the interpretation of experimental data; these include the site distribution (SD) model,[31, 39, 71] the non-equilibrium lattice fluid model (NELF) model,[97] and the unified dual mode model.[32] Due to their more realistic picture of microscopic aspects of permeation through glassy polymers, these models provide additional descriptions of the gas-polymer

system that could be useful for the interpretation of glassy polymer solubility and transport data at steady state. To fully understand the gas-polymer interactions under non-steady state conditions using these models, reaction-diffusion simulations like the ones presented in this paper will be required.

Conclusions

We report new gas permeation measurements for PPO by N_2 and CO_2 that provide time-dependent downstream pressure data for both steady and non-steady state regimes. Multiscale modeling incorporating physically-based reaction-diffusion kinetics and explicit gas uptake can reproduce the experimental data at steady and non-steady state using either single or dual mode transport models. Molecular dynamics simulations were performed to gain information on gas sticking to the PPO surface and show a sticking probability for CO_2 of 13%. Gas entry into the polymer is facile, so permeation is governed by polymer kinetics, not sticking. The equilibration between pressure and concentration in the polymer is not instantaneous; this slower polymer response must be included in the permeation mechanism to capture the pre-steady state behavior properly. Our findings along with other literature indicate that the common microscopic interpretation of the dual mode model is not self-consistent and does not explain the time-dependent permeation data for PPO. Rather, a molecular-level understanding of the diffusion process will serve to connect polymer structure to permeability, and to isolate polymer relaxation effects from specific chemical interactions that also influence permeation.

ASSOCIATED CONTENT

Supporting Information. A file containing supplementary information can be found at [link] containing the molecular metadynamics methods, additional details of the multiscale model implementation, methods for and effects of correction of sorption and permeation data for swelling, tables with all simulation inputs, plots of all permeation experimental data, literature data on permeability and solubility in PPO, analysis of the correlation of permeability with Tg and density, experimental permeability data with a linear fit, additional results of the molecular metadynamics simulations, additional single mode model results, and additional dual mode model results. Data used in this paper are available at [link].

AUTHOR INFORMATION

Corresponding Author * E-mail: fahoule@lbl.gov

Conflict of Interest Disclosure. The authors declare no competing interests.

Author Contributions. The initial plan for this study was conceived by MS and FH, and developed together with AW and WG. MT performed the experiments, and MS, DB, AM, NH, LW and BM performed the calculations. All authors contributed to the interpretation of the experimental, theoretical and multiscale modeling results and preparation of the manuscript. All authors have given approval to the final version of the manuscript.

Acknowledgements. The authors are grateful to Dr. Daniel J. Miller (JCAP, LBNL) for helpful discussions on membrane polymer science, and to Dr. William D. Hinsberg (Columbia Hill Technical Consulting) for discussions on the use of Kinetiscope in this work.

Funding Sources. This material is based upon work performed by the Joint Center for Artificial Photosynthesis, a DOE Energy Innovation Hub, supported through the Office of Science of the U.S. Department of Energy under Award Number DE-SC0004993. All experiments and multiscale modeling were performed in the Hub. M. T. thanks the National Science Foundation Graduate Research Fellowship under Grant No. DGE 1106400. D. B., N.H., B. M., and W. A. G. acknowledge funding from Bosch Energy Research Network Grant No 07.23.CS.15 for the MD simulation work. Bosch Energy Research had no involvement in decisions concerning data collection, data processing, writing, or article submission.

References

1. Hallinan, D. T.; Elabd, Y. A., Diffusion and Sorption of Methanol and Water in Nafion Using Time-Resolved Fourier Transform Infrared-Attenuated Total Reflectance Spectroscopy. *Journal of Physical Chemistry B* **2007,** *111* (46), 13221-13230.
2. Hallinan, D. T., Jr.; Elabd, Y. A., Sorption and Diffusion Selectivity. Kakaç, S.; Al, E., Eds. Springer: Dordrecht, 2008; pp 189-208.
3. Beckingham, B. S.; Lynd, N. A.; Miller, D. J., Monitoring Multicomponent Transport using In Situ ATR FTIR Spectroscopy. *Journal of Membrane Science* **2018,** *550*, 348-356.
4. DeLuca, N. W.; Elabd, Y. A., Polymer Electrolyte Membranes for the Direct Methanol Fuel Cell: A Review. *Journal of Polymer Science Part B: Polymer Physics* **2006,** *44*, 2201-2225.
5. Lewis, N. S.; Nocera, D. G., Powering the Planet: Chemical Challenges in Solar Energy Utilization. *Proceedings of the National Academy of Sciences* **2006,** *103* (43), 15729 LP-15735.
6. Crank, J.; Park, G. S., *Diffusion in Polymers*. Academic Press Inc., Ltd.: London and New York, 1968.
7. Wijmans, J. G.; Baker, R. W., The Solution-Diffusion Model: a Review. *Journal of Membrane Science* **1995,** *107*, 1-21.
8. Petropoulos, J.; Sanopoulou, M.; Papadokostaki, K., Beyond Fick: How Best to Deal with non-Fickian Behavior in a Fickian Spirit. *Diffusion Fundamentals* **2009,** *11* (5), 1-21.
9. Majsztrik, P. W.; Satterfield, M. B.; Bocarsly, A. B.; Benziger, J. B., Water Sorption, Desorption and Transport in Nafion Membranes. *Journal of Membrane Science* **2007,** *301* (1-2), 93-106.
10. Daly, K. B.; Benziger, J. B.; Panagiotopoulos, A. Z.; Debenedetti, P. G., Molecular Dynamics Simulations of Water Permeation across Nafion Membrane Interfaces. *Journal of Physical Chemistry B* **2014,** *118*, 8798-8807.
11. Soniat, M.; Houle, F. A., Swelling and Diffusion during Methanol Sorption into Hydrated Nafion. *The Journal of Physical Chemistry B* **2018,** *122* (34), 8255-8268.
12. Soniat, M.; Tesfaye, M.; Brooks, D.; Merinov, B.; Goddard Iii, W. A.; Weber, A. Z.; Houle, F. A., Predictive Simulation of Non-Steady-State Transport of Gases Through Rubbery Polymer Membranes. *Polymer* **2018,** *134*, 125-142.
13. Ghosal, K.; Freeman, B. D., Gas Separation Using Polymer Membranes: An Overview. *Polymers for Advanced Technologies* **1994,** *5* (11), 673-697.
14. White, R. P.; Lipson, J. E. G., Polymer Free Volume and Its Connection to the Glass Transition. *Macromolecules* **2016,** *49* (11), 3987-4007.
15. Shi, T.; Jiang, W.; An, L.; Li, B., Molecular Dynamics Simulation of Sub-Transition for Polyethersulfone. *Macromolecular Theory and Simulations* **2001,** *10* (4), 232-236.

16. Yampolskii, Y. P.; Pinnau, I.; Freeman, B. D., *Materials Science of Membranes for Gas and Vapor Separation*. John Wiley & Sons Ltd: West Sussex, England, 2006; p 445-445.
17. Sodaye, H. S.; Pujari, P. K.; Goswami, A.; Manohar, S. B., Probing the Microstructure of Nafion-117 Using Positron Annihilation Spectroscopy. *Journal of Polymer Science, Part B: Polymer Physics* **1997,** *35* (5), 771-776.
18. Goworek, T. Positronium as a Probe of Small Free Volumes in Crystals, Polymers and Porous Media. 2014.
19. Vrentas, J. S.; Vrentas, C. M., Sorption in Glassy Polymers. *Macromolecules* **1991,** *24*, 2404-12.
20. Maeda, Y.; Paul, D. R., Effect of Antiplasticization on Gas Sorption and Transport. II. Poly(phenylene Oxide). *Journal of Polymer Science: Part B: Polymer Physics* **1987,** *25*, 981-1003.
21. Bohlen, J.; Kirchheim, R., Macroscopic Volume Changes Versus Changes of Free Volume as Determined by Positron Annihilation Spectroscopy for Polycarbonate and Polystyrene. *Macromolecules* **2001,** *34* (12), 4210-4215.
22. Petropoulos, J. H., Quantitative analysis of gaseous diffusion in glassy polymers. *Journal of Polymer Science Part A-2: Polymer Physics* **1970,** *8* (10), 1797-1801.
23. Paul, D. R.; Koros, W. J., Effect of Partially Immobilizing Sorption on Permeability and the Diffusion Time Lag. *Journal of Polymer Science* **1976,** *14*, 675-685.
24. Chern, R. T.; Sheu, F. R.; Jia, L.; Stannett, V. T.; Hopfenberg, H. B., Transport of Gases in Unmodified and Aryl-Brominated 2,6-Dimethyl-1,4-Poly(Phenylene Oxide). *Journal of Membrane Science* **1987,** *35*, 103-115.
25. Bondar, V. I.; Kamiya, Y.; Yampol'skii, Y. P., On Pressure Dependence of the Parameters of the Dual-Mode Sorption Model. *Journal of Polymer Science, Part B: Polymer Physics* **1996,** *34* (2), 369-378.
26. Kanehashi, S.; Nagai, K., Analysis of Dual-Mode Model Parameters for Gas Sorption in Glassy Polymers. *Journal of Membrane Science* **2005,** *253* (1-2), 117-138.
27. Lo, C. H.; Hung, W. S.; De Guzman, M.; Huang, S. H.; Li, C. L.; Hu, C. C.; Jean, Y. C.; Lee, K. R.; Lai, J. Y., Investigation on CO2-Induced Plasticization in Polycarbonate Membrane Using Positron Annihilation Lifetime Spectroscopy. *Journal of Membrane Science* **2010,** *363* (1-2), 302-308.
28. Yuan, J.; Cao, H.; Hellmuth, E. W.; Jean, Y. C., Subnanometer Hole Properties of CO2-Exposed Polysulfone Studied by Positron Annihilation Lifetime Spectroscopy. *Journal of Polymer Science Part B* **1998,** *36*, 3049-3056.
29. Aitken, C. L.; Koros, W. J.; Paul, D. R., Effect of Structural Symmetry on Gas Transport Properties of Polysulfones. *Macromolecules* **1992,** *25* (13), 3424-3434.
30. Böhning, M.; Springer, J., Sorptive Dilation and Relaxational Processes in Glassy Polymer/Gas Systems-I. Poly(Sulfone) and Poly(Ether Sulfone). *Polymer* **1998,** *39* (21), 5183-5195.

31. Kirchheim, R., Sorption and Partial Molar Volume of Small Molecules in Glassy Polymers. *Macromolecules* **1992,** *25* (25), 6952-6960.
32. Guo, J.; Barbari, T. A., Unified Dual Mode Description of Small Molecule Sorption and Desorption Kinetics in a Glassy Polymer. *Macromolecules* **2009,** *42* (15), 5700-5708.
33. Houde, A. Y.; Kulkarni, S. S.; Kulkarni, M. G., Permeation and Plasticization Behavior of Glassy Polymers: A WAXD Interpretation. *Journal of Membrane Science* **1992,** *71* (1-2), 117-128.
34. Fried, J. R.; Sadat-Akhavi, M.; Mark, J. E., Molecular Simulation of Gas Permeability: Poly(2,6-Dimethyl-1,4-Phenylene Oxide). *Journal of Membrane Science* **1998,** *149* (1), 115-126.
35. Hofmann, D.; Fritz, L.; Ulbrich, J.; Paul, D., Molecular Simulation of Small Molecule Diffusion and Solution in Dense Amorphous Polysiloxanes and Polyimides. *Computational and Theoretical Polymer Science* **2000,** *10* (5), 419-436.
36. Hofmann, D.; Fritz, L.; Ulbrich, J.; Schepers, C.; Bhning, M., Detailed-Atomistic Molecular Modeling of Small Molecule Diffusion and Solution Processes in Polymeric Membrane Materials. *Macromolecular Theory and Simulations* **2000,** *9* (6), 293-327.
37. Hofmann, D.; Heuchel, M.; Yampolskii, Y.; Khotimskii, V.; Shantarovich, V., Free Volume Distributions in Ultrahigh and Lower Free Volume Polymers: Comparison Between Molecular Modeling and Positron Lifetime Studies. *Macromolecules* **2002,** *35* (6), 2129-2140.
38. Hölck, O.; Siegert, M. R.; Heuchel, M.; Böhning, M., CO2 Sorption Induced Dilation in Polysulfone: Comparative Analysis of Experimental and Molecular Modeling Results. *Macromolecules* **2006,** *39* (26), 9590-9604.
39. Neyertz, S.; Brown, D., Molecular Dynamics Study of Carbon Dioxide Sorption and Plasticization at the Interface of a Glassy Polymer Membrane. *Macromolecules* **2013,** *46* (6), 2433-2449.
40. Neyertz, S.; Brown, D., The Effect of Structural Isomerism on Carbon Dioxide Sorption and Plasticization at the Interface of a Glassy Polymer Membrane. *Journal of Membrane Science* **2014,** *460*, 213-228.
41. Toi, K.; Morel, G.; Paul, D. R., Gas Sorption and Transport in Poly(phenylene Oxide) and Comparisons with Other Glassy Polymers. *Journal of Applied Polymer Science* **1982,** *27*, 2997-3005.
42. Bondi, A., *Physical Properties of Molecular Crystals, Liquids and Glasses*. Wiley: New York, 1968.
43. Huang, Y.; Wang, X.; Paul, D. R., Physical Aging of Thin Glassy Polymer Films: Free Volume Interpretation. *Journal of Membrane Science* **2006,** *277* (1-2), 219-229.
44. *CRC Handbook of Chemistry and Physics: A Ready-Reference Book of Chemical and Physical Data.*
45. *Springer Handbook of Materials Measurement Methods*. Springer: Berlin, 2006; p 1207.

46. Wright, C. T.; Paul, D. R., Gas Sorption and Transport in UV-Irradiated Poly(2,6-dimethyl-1,4-phenylene oxide) Films. *Journal of Applied Polymer Science* **1998,** *67*, 875-883.
47. Shin, H.; Pascal, T. A.; Goddard, W. A.; Kim, H., Scaled Effective Solvent Method for Predicting the Equilibrium Ensemble of Structures with Analysis of Thermodynamic Properties of Amorphous Polyethylene Glycol-Water Mixtures. *Journal of Physical Chemistry B* **2013,** *117* (3), 916-927.
48. Plimpton, S., Fast Parallel Algorithms for Short-Range Molecular Dynamics. *Journal of Computational Physics* **1995,** *117*, 1-19.
49. Banks, J. L.; Beard, H. S.; Cao, Y.; Cho, A. E.; Damm, W.; Farid, R.; Felts, A. K.; Halgren, T. A.; Mainz, D. T.; Maple, J. R.; Murphy, R.; Philipp, D. M.; Repasky, M. P.; Zhang, L. Y.; Berne, B. J.; Friesner, R. A.; Gallicchio, E.; Levy, R. M., Integrated Modeling Program, Applied Chemical Theory (IMPACT). *Journal of Computational Chemistry* **2005,** *26* (16), 1752-1780.
50. Willard, A. P.; Chandler, D., Instantaneous Liquid Interfaces. *Journal of Physical Chemistry B* **2010,** *114* (5), 1954-1958.
51. Julin, J.; Shiraiwa, M.; Miles, R. E. H.; Reid, J. P.; Pöschl, U.; Riipinen, I., Mass Accommodation of Water: Bridging the Gap Between Molecular Dynamics Simulations and Kinetic Condensation Models. *Journal of Physical Chemistry A* **2013,** *117* (2), 410-420.
52. Julin, J.; Winkler, P. M.; Donahue, N. M.; Wagner, P. E.; Riipinen, I., Near-Unity Mass Accommodation Coefficient of Organic Molecules of Varying Structure. *Environmental Science & Technology* **2014,** *48*, 12083-12089.
53. Bowers, K.; Chow, E.; Xu, H.; Dror, R.; Eastwood, M.; Gregersen, B.; Klepeis, J.; Kolossvary, I.; Moraes, M.; Sacerdoti, F.; Salmon, J.; Shan, Y.; Shaw, D., Scalable Algorithms for Molecular Dynamics Simulations on Commodity Clusters. *ACM/IEEE SC 2006 Conference (SC'06)* **2006,** (November), 43-43.
54. Shivakumar, D.; Williams, J.; Wu, Y.; Damm, W.; Shelley, J.; Sherman, W., Prediction of Absolute Solvation Free Energies using Molecular Dynamics Free Energy Perturbation and the OPLS Force Field. *Journal of Chemical Theory and Computation* **2010,** *6*, 1509-1519.
55. Guo, Z.; Mohanty, U.; Noehre, J.; Sawyer, T. K.; Sherman, W.; Krilov, G., Probing the α-Helical Structural Stability of Stapled p53 Peptides: Molecular Dynamics Simulations and Analysis. *Chem. Biol. Drug Des.* **2010,** *75*, 348-359.
56. Bussi, G.; Donadio, D.; Parrinello, M., Canonical Sampling through Velocity Rescaling. *Journal of Chemical Physics* **2007,** *126* (1), 014101.
57. Essmann, U.; Perera, L.; Berkowitz, M. L.; Darden, T.; Lee, H.; Pedersen, L. G., A Smooth Particle Mesh Ewald Method. *Journal of Chemical Physics* **1995,** *103* (19), 8577–8593.
58. Pronk, S.; Páll, S.; Schulz, R.; Larsson, P.; Bjelkmar, P.; Apostolov, R.; Shirts, M. R.; Smith, J. C.; Kasson, P. M.; Van Der Spoel, D., GROMACS 4.5: A High-Throughput and Highly Parallel Open Source Molecular Simulation Toolkit. *Bioinformatics* **2013,** *29* (7), 845–854.

59. Abraham, M. J.; Murtola, T.; Schulz, R.; Páll, S.; Smith, J. C.; Hess, B.; Lindahl, E., GROMACS: High Performance Molecular Simulations through Multi-Level Parallelism from Laptops to Supercomputers. *SoftwareX* **2015,** *1*, 19–25.
60. Tribello, G. A.; Bonomi, M.; Branduardi, D.; Camilloni, C.; Bussi, G., PLUMED 2: New Feathers for an Old Bird. *Computational Physical Communications* **2014,** *185* (2), 604–613.
61. Hess, B., P-LINCS: A Parallel Linear Constraint Solver for Molecular Simulation. *Journal of Chemical Theory and Computation* **2008,** *4* (1), 116–122.
62. Bunker, D. L., Simple Kinetic Models from Arrhenius to the Computer. *Accounts of Chemical Research* **1974,** *7* (6), 195-201.
63. Bunker, D. L.; Garrett, B.; Kleindienst, T.; Long, G. S., Discrete Simulation Methods in Combustion Kinetics. *Combustion and Flame* **1974,** *23* (3), 373-379.
64. Gillespie, D. T., A General Method for Numerically Simulating the Stochastic Time Evolution of Coupled Chemical Reactions. *Journal of Computational Physics* **1976,** *22* (4), 403-434.
65. Kinetiscope. http://www.hinsberg.net/kinetiscope/, 2017.
66. Houle, F. a.; Hinsberg, W. D.; Morrison, M.; Sanchez, M. I.; Wallraff, G.; Larson, C.; Hoffnagle, J., Determination of Coupled Acid Catalysis-Diffusion Processes in a Positive-Tone Chemically Amplified Photoresist. *Journal of Vacuum Science & Technology B: Microelectronics and Nanometer Structures* **2000,** *18* (4), 1874-1874.
67. Atkins, P.; de Paula, J., *Physical Chemistry*. 8th ed.; W. H. Freeman and Co.: New York, USA, 2006.
68. Houston, P., *Chemical Kinetics and Reaction Dynamics*. DOVER PUBLICATIONS, INC.: Mineola, New York, 2001; p 48-49.
69. Somorjai, G. A.; Li, Y., *Introduction to Surface Chemistry and Catalysis*. Wiley: 2010; p 800-800.
70. Engel, T.; Reid, P., *Thermodynamics, Statistical Thermodynamics, & Kinetics*. 2nd ed.; Prentice Hall: 2010.
71. Gotthardt, P.; Grüger, A.; Brion, H. G.; Plaetschke, R.; Kirchheim, R., Volume Change of Glassy Polymers by Sorption of Small Molecules and its Relation to the Intermolecular Space. *Macromolecules* **1997,** *30* (25), 8058-8065.
72. Story, B. J.; Koros, W. J., Sorption and Transport of CO2 and CH4 in Chemically Modified Poly(Phenylene Oxide). *Journal of Membrane Science* **1992,** *67* (2-3), 191-210.
73. Aguilar-Vega, M.; Paul, D. R., Gas Transport Properties of Polyphenylene Ethers. *Journal of Polymer Science Part B: Polymer Physics* **1993,** *31* (11), 1577-1589.
74. Huang, Y.; Paul, D. R., Effect of MolecularWeight and Temperature on Physical Aging of ThinGlassy Poly(2,6-dimethyl-1,4-phenylene oxide) Films. *Journal of Polymer Science Part B: Polymer physics* **2007,** *45* (April), 1390-1398.

75. Tran, A.; Kruczek, B., Development and Characterization of Homopolymers and Copolymers from the Family of Polyphenylene Oxides. *Journal of Applied Polymer Science* **2007,** *106*, 2140-2148.
76. Maeda, Y.; Paul, D. R., Effect of Antiplasticization on Gas Sorption. III. Free Volume Interpretation. *Journal of Polymer Science: Part B: Polymer Physics* **1987,** *25*, 1005-1016.
77. Assogna, A.; Perego, G.; Roggero, A.; Sisto, R.; Valentini, C., Structure and Gas Permeability of Silylated Poly(Phenylene Oxide). *Journal of Membrane Science* **1992,** *71*, 97-103.
78. Jian, Z.; Xiaohuai, H., The Gas Permeation Property in Trimethylsilyl-Substituted PPO and Triphenylsilyl-Substituted PPO. *Journal of Membrane Science* **1994,** *97*, 275-282.
79. Alentiev, A.; Drioli, E.; Gokzhaev, M.; Golemme, G.; Ilinich, O.; Lapkin, A.; Volkov, V.; Yampolskii, Y., Gas Permeation Properties of Phenylene Oxide Polymers. *Journal of Membrane Science* **1998,** *138* (1), 99-107.
80. *Polymer Data Handbook*. Oxford University Press: 1999; p 1264-1264.
81. Kolb, C. E.; Cox, R. A.; Abbatt, J. P. D.; Ammann, M.; Davis, E. J.; Donaldson, D. J.; Garrett, B. C.; George, C.; Griffiths, P. T.; Hanson, D. R.; Kulmala, M.; McFiggans, G.; Pöschl, U.; Riipinen, I.; Rossi, M. J.; Rudich, Y.; Wagner, P. E.; Winkler, P. M.; Worsnop, D. R.; O'Dowd, C. D., An overview of current issues in the uptake of atmospheric trace gases by aerosols and clouds. *Atmospheric Chemistry and Physics* **2010,** *10* (21), 10561-10605.
82. Lancaster, D. K.; Johnson, A. M.; Burden, D. K.; Wiens, J. P.; Nathanson, G. M., Inert gas scattering from liquid hydrocarbon microjets. *Journal of Physical Chemistry Letters* **2013,** *4* (18), 3045-3049.
83. Lu, J. W.; Morris, J. R., Gas-Surface Scattering Dynamics of CO2, NO2, and O3 in Collisions with Model Organic Surfaces. *Journal of Physical Chemistry A* **2011,** *115*, 6194-6201.
84. Alexander, W. a.; Zhang, J.; Murray, V. J.; Nathanson, G. M.; Minton, T. K., Kinematics and Dynamics of Atomic-Beam Scattering on Liquid and Self-Assembled Monolayer Surfaces. *Faraday Discussions* **2012,** *157*, 355-374.
85. Donaldson, D. J., Adsorption of Atmospheric Gases at the Air−Water Interface. I. NH 3. *Journal of Physical Chemistry A* **1999,** *103* (1), 62-70.
86. COMSOL Multiphysics® v. 5.4. COMSOL AB, Stockholm, Sweden. www.comsol.com.
87. Chandler, D., *Introduction to Modern Statistical Mechanics*. Oxford University Press: Oxford, 1987; p 274.
88. Minelli, M.; Sarti, G. C., Permeability and Solubility of Carbon Dioxide in Different Glassy Polymer Systems with and without Plasticization. *Journal of Membrane Science* **2013,** *444*, 429-439.
89. Minelli, M.; Sarti, G. C., Gas transport in glassy polymers: Prediction of diffusional time lag. *Membranes* **2018,** *8* (1), 1-15.
90. Koros, W. J.; Chan, A. H.; Paul, D. R., Sorption and Transport of Various Gases in Polycarbonate. *Journal of Membrane Science* **1977,** *2*, 165-190.

91. McHattie, J. S.; Koros, W. J.; Paul, D. R., Effect of Isopropylidene Replacement on Gas Transport Properties of Polycarbonates. *Journal of Polymer Science: Part B Polymer Physics* **1991,** *29*, 731-746.
92. Aitken, C. L.; Koros, W. J.; Paul, D. R., Gas Transport Properties of Biphenol Polysulfones. *Macromolecules* **1992,** *25*, 3651-3658.
93. Erb, A. J.; Paul, D. R. *Gas Sorption and Transport in Polysulfone*; 1981; pp 11-22.
94. Breck, D. W., *Zeolite molecular sieves: structure, chemistry, and use*. R.E. Krieger: 1984.
95. Neyertz, S.; Brown, D., Oxygen Sorption in Glassy Polymers Studied at the Molecular Level. *Macromolecules* **2009,** *42* (21), 8521-8533.
96. Kupgan, G.; Demidov, A. G.; Colina, C. M., Plasticization behavior in polymers of intrinsic microporosity (PIM-1): A simulation study from combined Monte Carlo and molecular dynamics. *Journal of Membrane Science* **2018,** *565*, 95–103.
97. Doghieri, F.; Sarti, G. C., Nonequilibrium Lattice Fluids: A Predictive Model for the Solubility in Glassy Polymers. *Macromolecules* **1996,** *29* (24), 7885-7896.

1472 Table of Contents Graphic

1473

1474